Internship Final report

A digital twin for intelligent surfaces aided cellular network infrastructures leveraging Intelligent Reconfigurable Surfaces

Written by:
Yaacoub Yaacoub

Supervisors:
Prof. Chadi Barakat
Prof. Thierry Turletti
Prof. Damien Saucez

Abstract

The arrival of 5G and the emerging prospects of 6G wireless communication networks have necessitated innovative solutions to address the challenges posed by complex propagation environments, higher frequency usage, and increasing user demands. Intelligent Reconfigurable Surfaces (IRS) have emerged as a promising technology to enhance wireless communication systems by manipulating electromagnetic wave propagation. This report explores the significance of IRS in the context of modern wireless networks, particularly 5G and 6G, and presents a comprehensive simulator model for the design and analysis of IRS enabled environments. We will highlight first the critical role of IRS in overcoming propagation limitations, improving coverage, and enhancing capacity and energy efficiency in wireless networks.

With the increasing demands for higher data rates, low latency, and ubiquitous connectivity, IRS offers a revolutionary approach by leveraging its reconfigurable nature to adapt to varying propagation conditions, optimize signal quality, and reduce the need for deploying expensive additional base stations due to the higher attenuation of the spectrum in 5G and 6G. In addition, one of the most compelling advantages of IRS technology is its potential to enable wireless channel control, signifying a paradigm shift in wireless communication capabilities. Unlike traditional wireless environments, IRS equipped networks empower operators to actively manage and shape wireless channels according to their preferences. This new level of control introduces unprecedented opportunities for optimizing signal strength, minimizing interference, and tailoring wireless coverage to specific needs, which was previously infeasible.

In this report we will propose a new simulator model for RIS, implemented with varactor components for the signal elements of the surface. The simulator introduced will provide a precise framework for analyzing the performance of IRS in wireless communication scenarios. It offers a detailed understanding of the design considerations, simulation parameters, and mathematical derivations for IRS enabled systems. The model integrates factors such as transmitter-receiver geometry, incident and reflected signals trajectories based on a given frequency, and power calculations to evaluate the effectiveness of IRS in enhancing signal reception. The results obtained from the simulator reveal the remarkable potential of IRS in augmenting wireless communication systems. The model demonstrates the capability of IRS to improve the received signal power substantially, leading to substantial gains in signal quality and coverage. The calculated power gains underscore the efficacy of IRS in mitigating signal attenuation and multipath fading effects, especially in non-line-of-sight scenarios.

In conclusion, this report underscores the importance of Intelligent Reconfigurable Surfaces in shaping the future of wireless communication networks. The proposed simulator model serves as a valuable tool for comprehensively evaluating the impact of IRS on signal propagation, reception, and coverage enhancement. As 5G and 6G networks continue to evolve, IRS technology is ready to revolutionize wireless communication paradigms, offering unprecedented capabilities for dynamic wireless channel control, improved user experiences, and cost-effective network expansion.

Acknowledgment

This work was carried out during a 6-month internship at INRA, alongside team DIANA and the engineering faculty, Polytech Nice Sophia, at Université Côte d'Azur.

I would like to convey my deepest appreciation to my supervisors Chadi Barakat, Thierry Turletti and Damien Saucez who have spared no effort in enlightening me, providing their precious directions to ensure a smooth-running operation of the project and without ever failing to fulfill their duty of permanent availability.

I also wish to express my gratitude to them since they have given me the amazing opportunity to work on this wonderful project on the topic of Designing a simulator for an Intelligent Reconfigurable Surface, part of the CONVERGE European project that aims to develop of an innovative toolset combining radio and vision-based communications and sensing technologies enabling the emerging area of research aligned with the motto "view-to-communicate and communicate-to-view". This work pushed me to perform a lot of in-depth research about a variety of new related topics, utilizing my pre-existing skills in certain fields and developing new ones.

Table of Contents

Table of Figures

Table of Tables

A. Introduction

In the rapidly evolving landscape of wireless communication technology, a relentless drive to enhance network capacity and support higher data rates has led to innovative strategies that exceeded conventional boundaries. The quest for optimizing wireless performance, from ingenious modulation schemes to spatial diversity techniques like multiple-input multiple-output (MIMO), has explored every avenue [1]. Yet, the stochastic and unpredictable nature of wireless propagation, coupled with finite spectrum resources, remains a fundamental constraint. As a response to these challenges, the trajectory of wireless communication has embarked on a journey into higher frequency bands, venturing even into the millimeter-wave spectrum (30-100 GHz), a branch of untapped spectral potential. However, this climb into higher frequencies introduces a collection of unique propagation challenges, reshaping the dynamics of wireless communication. The established models that held authority at lower frequencies must now give way to the ascendancy of line-of-sight, first-order reflections, and scattering phenomena [2].

Emerging from this dynamic shift is a revolutionary concept: reconfigurable intelligent surfaces (RIS). Traditionally, wireless propagation and scattering elements were deemed uncontrollable, introducing unpredictability into the channel. RIS represents a paradigm shift, empowering the environment with a degree of control. This shift triggers a new concept of wireless system design, transforming once-uncontrollable environmental factors into system parameters that can be optimized to overcome the inherent problems of wireless communication [3]. The essence of RIS's potential lies in its dynamic alteration of wireless channel propagation characteristics. Through skillful manipulation of electromagnetic waves, RIS holds the promise of mitigating challenges stopping from shadowing, spatial multiplexing limitations, and adverse channel conditions. Specifically, scenarios burdened by weak signal strengths or sparse spatial multiplexing can be decisively reconfigured using RIS intervention. This transformation hinges on the central concept of leveraging RIS to steer signals, reshape reflections, and establish novel propagation pathways. Implementing RIS involves diverse methodologies, each offering distinct capabilities. Whether as dynamic reflectarrays or tunable metasurfaces, RIS introduces a spectrum of considerations, spanning from wave manipulation prowess to intricate channel modeling and link budget optimization [4].

The rise of RIS technology marks a new epoch in the wireless communication domain. Instead of solely relying on adaptive processing and modulation techniques to counter the stochastic nature of wireless channels, the communication environment itself becomes flexible. This shift empowers the environment as an integral element of the communication system, signaling opportunities to conquer the limitations that have long restricted wireless networks [2]. With the anticipation of 6G's transformative potential, the discourse inevitably turns to the future of current infrastructures and their alignment with forthcoming technological standards. While 6G remains unstandardized, it's projected to reshape wireless communication, necessitating efficiency for real-time communication, pervasive intelligence, and ubiquitous connectivity. As applications diversify, the challenges associated with the high-frequency mm-wave and THz frequency range come to the face, demanding solutions to issues such as obstacles, blockages, limited coverage, and path loss. In this landscape, reconfigurable intelligent surfaces (RIS) emerge as a promising solution. By enabling virtual line-of-sight propagation paths, RIS installed on flat surfaces holds the potential to mitigate challenges associated with the new applications and services anticipated in the 6G era. A transformative technology, RIS reshapes wireless communication paradigms and addresses a range of challenges, sparking further exploration into its benefits and use cases [5]. The evolution from 5G to 6G entails a shift from enhancing transmitter and receiver functionalities to smart

propagation environments. RIS, utilizing cost-effective passive devices, possesses the potential to facilitate this transformation. The convergence of computer vision and wireless communication in the beyond 5G/6G landscape further emphasizes the significance of RIS. While configuring meta-surfaces in real-time remains a challenge, leveraging computer vision and learning approaches can enhance efficiency and real-time configuration, catering to dynamic scenarios with moving obstacles and users.

In this context, the preliminary phase involves studying a model to control incident wave properties, enabling different angle reflections. This foundation will pave the way for more complex experiments using a digital twin, simulating experiments on a larger scale. Although challenges abound, the exploration of RIS's capabilities to manipulate wave propagation offers exciting possibilities, both with and without the aid of machine learning and deep learning. As the landscape evolves, the intrigue surrounding RIS and its potential to reshape wave propagation continues to grow.

This report aims to illuminate the novel IRS technology. Beginning with a theoretical overview grounded in existing literature, presenting its necessity in the future generation networks that will be explained in the 5G and 6G overviews paragraphs. Following this, I will reveal the fundamental scientific concepts that underpin the realization of this innovation from radio waves to electronic circuitry. Once these foundational aspects are comprehended, I will explore the intricate details of IRS development and expound on its technical mechanisms presenting its working principles and a signal perspective overview of systems dealing with IRS and then show some of its expected usage in the future. Moving forward, I will define the global framework of our work that lies in the CONVERGE project. Then I will continue with the introduction of our proper IRS model simulator design and provide an exposition of the results it has yielded. Concluding the discussion, I will conduct a comprehensive evaluation of the simulator's strengths and weaknesses. By identifying its limitations, I will plan a course for future work aimed at rectifying these limitations and driving the technology towards greater efficacy and applicability.

1. 5G Overview

In today's rapidly evolving technological landscape, the prevailing network technology that underpins our digital interactions is the peak of numerous advancements and iterations. During this progression, the adoption of various generations, from 2G to 4G, has brought us closer to realizing the promise of seamless connectivity and transformative capabilities. However, as we stand on the precipice of a new era, the spotlight now shifts to the fifth generation of wireless technology, commonly known as 5G. This paradigm shift holds the potential to revolutionize our communication landscape, introducing a complex architecture that goes beyond the conventional while weaving in innovative concepts like network slicing, cloud-native design, and edge computing.

In this context, let's dip into the multifaceted architecture of 5G networks and explore how it forms the basis of unprecedented connectivity and possibilities. The architecture of 5G networks is a carefully designed framework forming the backbone of the fifth generation of wireless technology. It's divided into two primary subsystems: the Radio Access Network (RAN) and the Mobile Core. The RAN, composed of strategically positioned gNBs (gNodeBs), acts as the intermediary between user devices and the network. It employs advanced techniques such as massive Multiple-Input Multiple-Output (MIMO) and beamforming to amplify coverage, capacity, and overall performance [39]. These gNBs establish wireless communication with user devices, ensuring seamless coverage across diverse environments. They efficiently manage radio resources, enforce Quality-of-Service (QoS) policies, and coordinate cell handovers for uninterrupted connectivity and optimized performance [39].

Conversely, the Mobile Core, also known as the core network, is instrumental in enabling various services and functionalities. It encompasses multiple network functions providing services like connectivity management, data routing, and security. This core network evolved through concepts like Network Function Virtualization (NFV) and Software-Defined Networking (SDN), enhancing flexibility, scalability, and resource allocation [39].

An innovative concept enabled by 5G architecture is network slicing. It logically divides the physical network into virtual networks or "slices," each optimized for specific service requirements. This feature benefits applications like IoT, ultra-reliable services, and high-speed broadband, coexisting on the same infrastructure while maintaining isolation and tailored performance. The architecture fully embraces cloud-native principles, deploying modular network functions in cloud environments for rapid deployment, scalability, and efficient resource usage. Edge computing is seamlessly integrated, reducing latency and enhancing real-time application experiences for AR, industrial automation, and autonomous vehicles. Security is vital in 5G architecture, with enhanced mechanisms including authentication, encryption, and network slicing isolation to safeguard user data and network integrity. In brief, 5G network architecture intricately blends the Radio Access Network, the Mobile Core, network slicing, cloud-native design, edge computing, and robust security. This structure enables 5G to cater to various applications, positioning it as the foundation of our interconnected world. 5G's advent marks a transformative era in wireless communication, driving changes across industries and societies.

As the fifth generation, 5G builds on its predecessors, aiming for unparalleled connectivity and performance. This journey is a fusion of diverse techniques, scenarios, and use cases to meet modern communication demands. At its core, 5G's ambitious objectives surpass 4G capabilities. It elevates data capacities for applications like UHD streaming and IoT, raising user data rates tenfold to a hundredfold. Accommodating more devices (up to ten times) is vital for IoT in smart environments. Beyond speed, 5G enhances user experience, prolonging IoT device battery life and significantly reducing end-to-end latency, empowering real-time applications like AR and remote surgery. This evolution is driven by initiatives like METIS, 5GNOW, and collaboration with industry leaders. 5G reshapes industries like healthcare and entertainment, unlocking new opportunities [6].Lastly, 5G technology shifts connectivity, empowering smart cities and ubiquitous experiences. It involves research, development, and collaboration, realizing transformative potential. Also, 5G's implementation incorporates SDN and NFV, creating specialized network slices. The 5G cellular network includes RAN and the Mobile Core. The former manages radio spectrum based on QoS, while the latter enables seamless connectivity and efficient billing [6].

2. 6G Overview

In a time when technology keeps advancing, wireless communication is growing fast. With each new version, it's opening up new possibilities. The next big step is 6G wireless, which has caught the attention of researchers, inventors, and industry leaders. This upcoming advancement in connectivity will not be a small improvement only, instead, it's going to completely change how technology is used and how people will connect in the future.

While 6G's initial status naturally veils it in an air of anticipation, an article written by Harsh et. al has surfaced, offering insights into the potential architectural landscapes and applications that could characterize this paradigm-shifting generation of wireless communication. Embedded within the blueprint of the envisioned 6G view is an architecture that harmonizes leading-edge technologies to establish an uninterrupted bridge between the digital and physical words. In 6G, researchers are envisioning the

integration of terahertz frequencies, the augmentation of advanced massive MIMO (Multiple-Input, Multiple-Output) systems, and the fusion of terrestrial and satellite networks. This combination is set to create extremely fast and unprecedented data speeds, remarkably low latency, and unparalleled reliability, thus serving as the basis upon which plenty of transformative applications may be built. Within this complex framework lies an expanse of potential applications that extend beyond the limits of conventional communication. 6G comes as a sign that we're moving beyond the limits of its earlier versions, ushering in an era where augmented reality (AR) and virtual reality (VR) experiences attain true immersion, the internet will mix physical touch with digital interactions, and remote holography offers new possibilities. To make all these different uses work well, we need a flexible and adaptable network architecture that can handle all these different needs smoothly [7].

However, like any ambitious technological leap, the journey toward manifesting the 6G vision is loaded with tough challenges that necessitate innovative competence and cooperation. The intricate complexities associated with harnessing terahertz frequencies pose substantial obstacles, encompassing considerations of propagation and penetration that demand pioneering beamforming techniques. Moreover, making different services work well together and handling a huge number of connected devices requires new ways to decide who gets to use which parts of the wireless spectrum and how resources are managed. These are important for 6G networks to work effectively. In short, the upcoming arrival of 6G wireless systems is ready to change how we think about connectivity [7]. Although it might seem mysterious and uncertain, taking a closer look gives us hints about possible ways these networks could be designed and used. Mixing different technologies, expanding how we use them, and facing the challenges together give us a clear picture of where 6G networks might be headed. As we're on the edge of this new technological era, moving towards 6G will be more than just better connections, it will be about changing how we see our digital future.

When thinking about where Reconfigurable Intelligent Surface (RIS) technology fits in, it's important to look at how 6G is developing now. This helps us understand what role RIS might play in the future of networks. Despite the evolving nature of 6G, preliminary insights into key performance indicators (KPIs) and potential technologies have emerged. With growing applications like artificial intelligence (AI), virtual reality (VR), 3D media, and the Internet of Everything (IoE), the demand for connectivity surges, fueled further by the rise of autonomous systems across sectors [8]. While 5G networks are unfolding globally, limitations in realizing fully automated intelligent networks and immersive experiences persist, highlighting the significance of 6G as the next mobile network iteration. Envisioned as an extension of 5G capabilities, 6G seeks to provide even faster, more reliable communication with lower latency, necessitating innovative technologies like RIS. The specifics of 6G are still unfolding, with advanced radio frequencies from 30 to 300 GHz, including mmWave and potentially up to THz frequencies [7], anticipated for achieving faster data rates. Given the challenges associated with higher frequencies, including obstacle sensitivity, technologies like RIS become critical for unlocking 6G's potential.

B. Useful Concepts

1. Radio Waves

To understand the working principle of the RIS, we need first to have a good grasp of the physical properties and the phenomena that inspired and allowed the existence of such technology.

As we saw earlier, RIS main functionality is to handle incoming radio waves in a controllable way. To do so, we need to understand first what a radio wave is and how it is defined. Radio waves are one kind of electromagnetic wave generated using specialized antennas connected to radio transmitters. The transmitter applies changing electric currents to the antenna, causing it to emit radio waves. These waves are captured by receiving antennas connected to radio receivers. When radio waves interact with the receiving antenna, they induce oscillating currents, which are then detected by the receiver. These waves are portrayed as a series of repeating patterns of peaks and valleys. This entire pattern, which occurs before the repetition, is called a cycle. These waves are characterized by their wavelength, frequency, polarization, and intensity. The wavelength is the distance taken by a wave to complete one full cycle. The frequency refers to the number of cycles a wave completes in a single second and is measured in hertz (Hz), which quantifies cycles per second. The velocity of electromagnetic waves will depend on the medium in which they are travelling. Each medium is defined by a refractive index defining how much the travelling electromagnetic wave will be slowed down in the medium compared with free space. For free space, the refractive index is 1 where we get the base speed of light that we know, $c = 299{,}792{,}458\ \mathrm{m/s}$. The relationship between the velocity of the wave and the speed of light is:

$$\eta = \frac{c\ (m/s)}{v\ (m/s)} \tag{1}$$

Where:
η is the refractive index on a medium
c is the speed of light equal to $299{,}792{,}458\ \mathrm{m/s}$
v is the speed of the wave in the medium

The frequency of the electromagnetic wave is defined as:

$$f(Hz) = \frac{v\ (m/s)}{\lambda\ (m)} \tag{2}$$

As we can see, the relationship between the frequency and the wavelength in inversely proportional meaning that low frequency waves will have long wavelengths, and high frequency waves will have short wavelengths. This concept is so important in the context of RIS since it is one of the fundamental reasons supporting its creation. The span of the radio spectrum is recognized to extend from 3 kHz to 300 GHz. As for what concerns us in this project, we are considering the electromagnetic waves used in the communication environment, so the travel medium is always air which can be considered as free space medium in which the travelling speed of the electromagnetic wave will be c. In this case the wavelength-frequency relationship will be:

$$f(Hz) = \frac{c\ (m/s)}{\lambda\ (m)} \tag{3}$$

The next characteristic of an electromagnetic wave is polarization which is a concept that describes the orientation of a radio wave's electric field as it stands perpendicular to the wave's movement. A radio wave can be plane polarized, meaning its electric field oscillates along a specific plane in line with its motion. If the electric field oscillates horizontally, it's called a horizontally polarized wave. Conversely, if the oscillation is vertical, it's termed a vertically polarized wave. A circularly polarized wave exhibits a unique behavior, where its electric field rotates around the direction of travel once per cycle. A right circularly polarized wave follows a clockwise rotation, while a left circularly polarized wave rotates counterclockwise. Importantly, the wave's magnetic field is at a right angle to the electric field, and both fields align in a right-hand configuration concerning the direction of radiation.

Finally, the intensity of the wave is defined by the power of the signal per unit area and expressed in (w/m^2).

Radio waves are extensively utilized for communication due to their unique ability to travel through various barriers and environments, making them particularly effective for practical radio systems. This advantage arises from their extended wavelength. Radio waves can easily penetrate the atmosphere regardless of weather conditions and most of the obstacles. They also exhibit the capacity to bend around obstacles through a phenomenon called diffraction and tend to scatter rather than get absorbed by objects larger than their wavelength.

The propagating radio waves encounter various interactions like reflection, refraction, polarization, diffraction, and absorption. Different frequencies experience these interactions in different manners, making specific radio bands more suitable for particular applications. For radio communication two propagation methods are utilized:

Line of sight: This involves direct transmission from a sending antenna to a receiving antenna. Even though a clear line of sight is not always necessary, lower-frequency radio waves can pass through buildings and other barriers. Common uses for line-of-sight propagation include cell phones, FM radio, television broadcasting, and radar. Point-to-point microwave relay links also utilize this method by transmitting microwaves through dish antennas to cover long distances up to the visual horizon.

Indirect propagation: Radio waves can reach locations beyond direct line of sight through diffraction and reflection. Diffraction allows radio waves to curve around objects like buildings or vehicles, while surfaces such as walls, floors, and the ground partially reflect the waves. This mode is employed in short-range communication systems like cell phones, cordless phones, walkie-talkies, and wireless networks. This is the area where the RIS will come to play, controlling these behaviors to make them more efficient and useful [40].

2. Electronic Circuits

Manipulating the radio waves reflections using Reconfigurable Intelligent Surfaces (RIS) will involve the adjustment of the electronic characteristics of the components making up the metasurfaces. A single element of the RIS could be modeled with some basic electronic components such as resistors R (in Ω), capacitors C (in F), inductors L (in H), and diodes. In circuits theory, when a circuit is composed of a combination of these components, each one will be defined by its corresponding impedance and then merged together to find the equivalent impedance for the whole circuit which is given as follows.

$$Z = R + jX \tag{4}$$

Where R represents the real component of impedance, indicating resistance which is an electrical property that quantifies the opposition encountered by an electric current as it flows through a material or component. It is measured in ohms (Ω). The resistive losses refer to the dissipation of energy primarily as heat.

X is the Imaginary part of the impedance, representing reactance. Reactance is a measure of how a component stores and releases energy in response to AC. It's influenced by factors like capacitance and inductance. To calculate the reactance (X) of a circuit, you need to know the frequency of the alternating current (AC) signal and the type of circuit element you're dealing with such as inductors or capacitors or combination of both and calculate first the reactance of these components.

The reactance of an inductor is given by the formula:

$$X_L = j\omega L \tag{5}$$

The reactance of a capacitor is given by the formula:

$$X_C = \frac{1}{j\omega C} \tag{6}$$

Where L is the inductance of the coil or inductor element of the circuit. This measure represents the ability of the coil to store energy in the form of a magnetic field when an electric current flows through it. It is measured in Henrys (H).

C is the Capacitance of the capacitor element of the circuit. This measure represents the ability of the element to store to electric charge when a voltage difference exists across it. It is measured in Farads (F).

ω represents the angular frequency of the circuit. It is used to describe the rate of change of a sinusoidal waveform. The angular frequency is related to the regular frequency (f) of the waveform by the equation:

$$\omega = 2\pi f \tag{7}$$

Noting that reactance is a quantity that indicates the opposition offered to the flow of AC by capacitive or inductive elements. It behaves differently from resistance (R) in that it doesn't involve energy loss through heat. Instead, it's related to the phase relationship between voltage and current in AC circuits.

Finally, after calculating the individual impedances of each element of the circuit, finding the equivalent impedance in not more than a matter of the application of the series or parallel rules: Depending on whether the circuit elements are connected in series or parallel, apply the appropriate rules. For series connections, sum up the individual impedances.

$$Z_{total} = Z_1 + Z_2 + \cdots + Z_n \tag{8}$$

For parallel connections, use the reciprocal rule:

$$\frac{1}{Z_{total}} = \frac{1}{Z_1} + \frac{1}{Z_2} + \cdots + \frac{1}{Z_n} \tag{9}$$

and then take the reciprocal of the result to get the total impedance.

Going back to the context of our topic, the earlier-derived equivalent circuit impedance finds application in evaluating the reflection coefficient at the interface between the surface and free space. This

coefficient's value is influenced by the refractive indices or impedances of the media involved. A foundation of optics, microwave engineering, and other wave propagation domains, it provides profound insights into interactions with material interfaces, quantifying the proportion of incoming electromagnetic energy that reflects upon encountering refractive index or impedance shifts between media. The coefficient signifies the interface's proficiency in reflecting incoming waves and constitutes a pivotal tool for characterizing electromagnetic wave behavior at such boundaries.

This reflection coefficient will be calculated as follows:

$$\Gamma = \frac{Z_n - Z_0}{Z_n + Z_0} \tag{10}$$

Where:

- Z_0 is the impedance of free space which is a fundamental electromagnetic property that characterizes how electromagnetic waves propagate through empty space. It is a constant that represents the ratio of the electric field strength to the magnetic field strength in a propagating electromagnetic wave.

$$Z_0 = \sqrt{\frac{\mu_0}{\epsilon_0}} \approx 377\Omega \tag{11}$$

- Z_n is the electrical impedance of the element.

The incorporation of reactive elements into the circuit will result in a complex number representation for the reflection coefficient. In this case Γ can have a more useful representation in our context.

$$\Gamma = A_n e^{j\phi_n} \tag{12}$$

Where:

- A_n is the amplitude of the reflection coefficient Γ which practically will be in the range $[0, \dots, 1]$ and considered as the resistive loss that the signal will endure when hitting a given element.
- ϕ_n is the phase shift.

C. Reconfigurable Intelligent Surface

1. IRS Formal Definition and working Principle

As the landscape of wireless communication evolves with the emergence of 5G and the anticipated arrival of 6G networks, the demand for innovative solutions to enhance network performance and efficiency becomes increasingly evident. Reconfigurable Intelligent Surfaces (RISs) have emerged as a groundbreaking technology that holds promise in meeting these evolving needs. These intelligent surfaces represent a paradigm shift in wireless communication by introducing programmable and controllable channels in a wireless environment. A Reconfigurable Intelligent Surface (RIS) is an emerging concept rooted in extensive research within electromagnetic fields and wave propagation. This innovative idea holds great promise for reshaping wireless communication landscapes [9]. Essentially, an RIS comprises an array of individual, controllable elements that collectively offer the ability to manipulate incoming electromagnetic waves. These elements, while remaining passive, can be dynamically adjusted in response to external signals or commands [2], [10]. Although the terminology for this technology varies, encompassing designations like software-controlled metasurfaces and intelligent reflecting surfaces [9], the core principle remains consistent. RIS occupies a unique space between transmitters and receivers, effectively altering the behavior of wireless propagation environments [2], [10]. The technological realization of RIS can take diverse forms, yet metasurfaces, which consist of subwavelength unit cells, emerge as a prominent implementation choice [10], [11]. These unit cells, though small in comparison to the wavelength of electromagnetic waves, collectively allow for beam manipulation when combined with appropriate signal processing techniques. This innovation has the potential to revolutionize wireless communication by enabling the redirection and concentration of signals in specific directions [10]. The practical implications of RIS extend far beyond its technological complexity, introducing novel signal processing challenges. Consequently, existing communication models must be reexamined and adapted to accommodate this transformative technology [9]. In essence, RIS offers a groundbreaking shift in how wireless signals are managed and propagated. By harnessing passive elements that can be dynamically reconfigured, RIS introduces a level of control and adaptability that was previously unattainable. This innovative concept, nurtured by decades of electromagnetic research, underscores the evolving nature of wireless communication technologies [2]. As RIS continues to develop and find practical applications, it not only promises to enhance signal quality and coverage but also challenges us to rethink the fundamental principles of wireless communication [9].

The domain of Reconfigurable Intelligent Surfaces (RISs) encompasses a diverse array of implementations, ranging from active to passive configurations. These variations include smart surfaces that possess the capability to amplify and engage in signal processing operations on incoming radio waves, thereby introducing the concept of active RISs. Active RISs are characterized by their ability to generate and receive radio signals, necessitating an active RF chain for each active antenna element. These systems offer active transmission beamforming, which extends their capabilities beyond passive counterparts. On the other hand, passive RISs excel in their minimalist approach. They refrain from power amplification and elaborate signal processing, instead opting for passive reflection beamforming to manipulate wireless propagation. This passive approach aligns with the criteria of nearly passive and dynamic RISs, as they exclusively consume minimal power during the configuration phase. The categorization between active and passive RISs underscores the adaptability of this technology, accommodating both configurations based on specific use cases and desired functionalities. Moreover, the classification extends to the distinction between static

and dynamic/reconfigurable surfaces, each with unique implications. While active RISs introduce amplification and sophisticated processing into the wireless environment, passive counterparts concentrate on manipulation without power enhancement, positioning them as integral components of the expanding field of wireless communication research and implementation.

Reconfigurable Intelligent Surfaces (IRS) represent a groundbreaking advancement in wireless communication, addressing the evolving needs of 5G and 6G networks. These smart surfaces offer the fascinating ability to dynamically control the reflection of radio waves, presenting a new paradigm for enhancing wireless connectivity. The IRS consists of a surface partitioned into numerous small elements, each purposefully designed to be smaller than the wavelength (λ) of the incident electromagnetic wave. This size criterion is essential, as it enables the surface to exert precise control over the reflected signals. The property of an IRS lies in its element-level independence, granting it the power to plan sophisticated manipulations of electromagnetic properties at a granular level. The operation of an IRS is characterized by its energy efficiency, requiring minimal power consumption even as it exerts complicated control over the signal reflections.

The fundamental building blocks underlying an IRS's operation are Varactor Diodes or PIN Diodes, which serve as dynamic components facilitating the reconfiguration of the surface's electromagnetic characteristics. This dynamic adaptability is central to the functioning of the IRS, allowing it to harness a wide range of reflection patterns in response to varying needs and scenarios. The core working principle of an IRS revolves around altering the direction of incoming signals through the manipulation of their phase. The link between the phase change and the direction is governed by the Modified Snell's Law, a fundamental principle that governs the bending of waves at the interface between different media. By emulating a curved surface, the metasurface introduces tailored phase shifts across its area. This phase engineering introduces a crucial variability that underpins the IRS's ability to redirect signals to desired locations.

The successful operation of the IRS rests on the synchronization of these phase shifts at the receiver end. To ensure focused signal reception, it is imperative that the total delay of the signal is consistent across all surface elements. This synchronization is achieved through an interplay of phase adjustments, which collectively steer the signal toward the intended location. Critically, the phase shifts are manifest as changes in the reflection coefficients of the individual elements. The calculation of these coefficients involves complex numbers, denoted as $A_n e^{i\phi_n}$, with A_n representing the amplitude or signal attenuation coefficient, and ϕ_n signifying the actual phase shift of the element. Thus, the dynamic manipulation of the signal's phase is synonymous with modulating the electrical impedance of each element, an action that fundamentally defines the IRS's capacity for precise signal control.

In summary, Reconfigurable Intelligent Surfaces offer an ingenious solution to the challenges posed by modern wireless communication. These smart surfaces leverage their independent elements, energy-efficient operations, and phase manipulation to facilitate controlled signal reflection. As 5G and 6G networks continue to shape the future of wireless communication, the ability of IRS to completely change how we connect is ready to have a very important role.

2. Signal Processing Perspective

Considering in this case that we have a planar IRS surface having N elements with a line of sight to both the transmitter and the receiver having both a single antenna transmitting and receiving signals at a given carrier frequency f_c.

We will denote by:

- $x(t)$ the signal to be transmitted.
  - $x(t)e^{j2\pi f_c t}$ is the signal transmitted
- Channel modeled between the transmitter and the surface as $h_{1,n} = \alpha_{1,n}e^{-j\varepsilon_{1,n}}$ for each element n of the metasurface.
  - $\alpha_{1,n}$ amplitude attenuation of the channel
  - $\varepsilon_{1,n}$ phase shift of the channel

Then the signal reaching an IRS element will be given a follow:

$$y_{in,n}(t) = \alpha_{1,n}e^{-j\varepsilon_{1,n}}x(t)e^{j2\pi f_c t} \tag{13}$$

We then denote the Attenuation and the phase shift of the IRS by β_n and ϕ_n respectively.

Then we will have the signal just after its reflection by the IRS as:

$$y_{out,n}(t) = \beta_n e^{j\phi_n}\alpha_{1,n}e^{-j\varepsilon_{1,n}}x(t)e^{j2\pi f_c t} \tag{14}$$

At the receiver, we will add to $y_{out,n}(t)$ the channel between the surface and the receiver modeled as $h_{2,n} = \alpha_{2,n}e^{-j\varepsilon_{2,n}}$ for each element n of the metasurface.

  - $\alpha_{2,n}$ amplitude attenuation of the channel
  - $\varepsilon_{2,n}$ phase shift of the channel

So finally, the received signal will take the following form:

$$y_{r,n}(t) = \beta_n e^{j\phi_n}\alpha_{1,n}e^{-j\varepsilon_{1,n}}\alpha_{2,n}e^{-j\varepsilon_{2,n}}x(t)e^{j2\pi f_c t} \tag{15}$$

Or

$$y_{r,n}(t) = \beta_n e^{j\phi_n}h_{1,n}h_{2,n}x(t) \tag{16}$$

Summing up all the signals at the receiver we will have the resultant received signal:

$$y(t) = \sum_{n=1}^{N} \beta_n e^{j\phi_n}h_{1,n}h_{2,n}x(t) \tag{17}$$

Or

$$y(t) = H_1 \Phi H_2 x(t) \tag{18}$$

Where:

- $H_1 = [h_{1,1}, \dots, h_{1,N}]$
- $H_2 = [h_{2,1}, \dots, h_{2,N}]^T$

- $\Phi = diag\left(\beta_1 e^{j\phi_1}, \dots, \beta_N e^{j\phi_N}\right)$

It's important to note that the characteristics of the channel coefficients $H_1$and H_2 generally depend on distance-related path loss, large-scale shadowing, and small-scale multipath fading [2].

Considering the distances between the transmitter, the receiver and the RIS surface as d_t and d_r, the power received by the receiver will be proportional to the square of the distances.

$$P_r \propto \frac{1}{(d_t + d_r)^2} \tag{19}$$

This happens because the IRS reflected channel via the n elements will suffer from double path loss known as the product-distance pathloss model. Consequently, in practical scenarios, an IRS with a large number of elements is needed to compensate for this severe power loss. This can be accomplished by cohesively optimizing the reflection amplitudes and phases of these elements to attain notable gains in passive beamforming [2]. From this discussion, one can ask the question about the natural relation between the power and the number of elements. Does it grow linearly with the number of elements N, or there is a theoretical limit relating these two quantities. To answer this question accurately we need an exact model of the channel gain. Björnson et al in their paper, *Power Scaling Laws and Near-Field Behaviors of Massive MIMO and Intelligent Reflecting Surfaces*, answered this question by deriving an exact model of the channel gain given as

$$\alpha_{d,n} = \frac{N\beta_d}{3(N\beta_d\pi + 1)\sqrt{2N\beta_d\pi + 1}} + \frac{2}{3\pi}\tan^{-1}\left(\frac{N\beta_d\pi}{\sqrt{2N\beta_d\pi + 1}}\right) \tag{20}$$

Where:

$\beta_d = \frac{A}{4\pi d^2}$ *the free space channel gain*

N *is the total number of elements of the surface*

Using this channel gain model, they proved that in the best cases, with $N \to \infty$, the power received will saturate at one third of the transmitted power which satisfies the law of conservation of energy.

$$P_{rx} = \frac{P_{tx}}{3} \tag{21}$$

An intuitive explanation for why the limit is finite, despite the array's infinite size, is that each new receive antenna is deployed further away from the transmitter; the effective area which is perpendicularly to the direction of propagation becomes gradually smaller and the polarization loss also increases [13].

3. Wave Optics and Ray Optics analysis perspective

The interaction analysis between a Reconfigurable Intelligent Surface (RIS) and incident electromagnetic (EM) waves can be approached through two primary methodologies: ray-optics and wave-optics. These methods, while based on approximations, provide valuable insights into wave-material interactions. Both are frequently employed in RIS literature yet differ in their assumptions and interpretations. In ray-optics analysis is built upon Snell's laws, EM waves are represented as rays with varying phases, progressing linearly based on optical path length. The interaction with materials is explored through phase changes and refractive indices. Co-phase conditions determine desirable reflected waves. Wave-optics views EM waves as electric and magnetic fields, characterized by complex-valued vectors denoting amplitude, phase, and direction. Wavefronts, surfaces with equal phase values, guide interaction analysis, enabling proper transformations for obtaining desired scattered waves via the RIS. Waves-optics relies on Maxwell's Equations when analyzing the surface behavior. While these approaches differ in perspective, they collectively contribute to comprehending the complex interactions between RIS and EM waves [10].

4. IRS electronic Models

As we mentioned earlier, to enable signal redirection control and beam forming, multiple techniques, the main three approaches proposed in the literature are the following; 1) mechanical manipulation involving actions like mechanical rotation and translation, 2) utilization of functional materials such as liquid crystals and graphene, and 3) implementation of electronic components like positive-intrinsic-negative (PIN) diodes, varactor diodes, field-effect transistors (FETs), or micro-electromechanical system (MEMS) switches. Practically, the third approach has been widely adopted for real physical implementation due to its fast response time, low reflection loss as well as relatively low energy consumption and hardware cost [2]. The main components used are the Varactor Diodes and the Positive-Intrinsic-Negative (PIN) Diodes. In the following, we will present the working principle of each implementation, presenting its advantages and inconveniences.

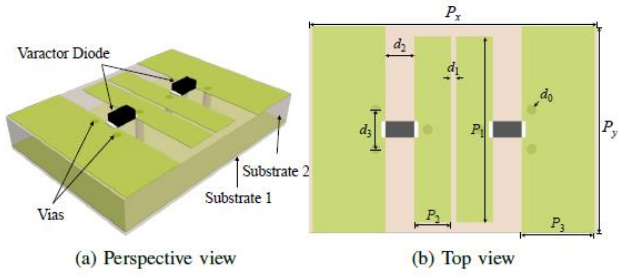

Figure 1: Element model with Varactor Diode [12]

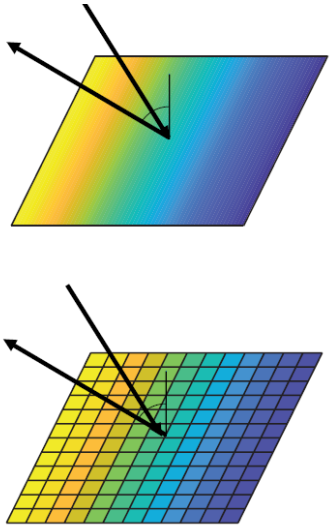

Figure 2: IRS using elements with varactors trying to emulate a smooth surface phase shift. upper figure showing theoretical phase shift for the surface. Lower figure showing the phase shifts created by the elements with varactor.

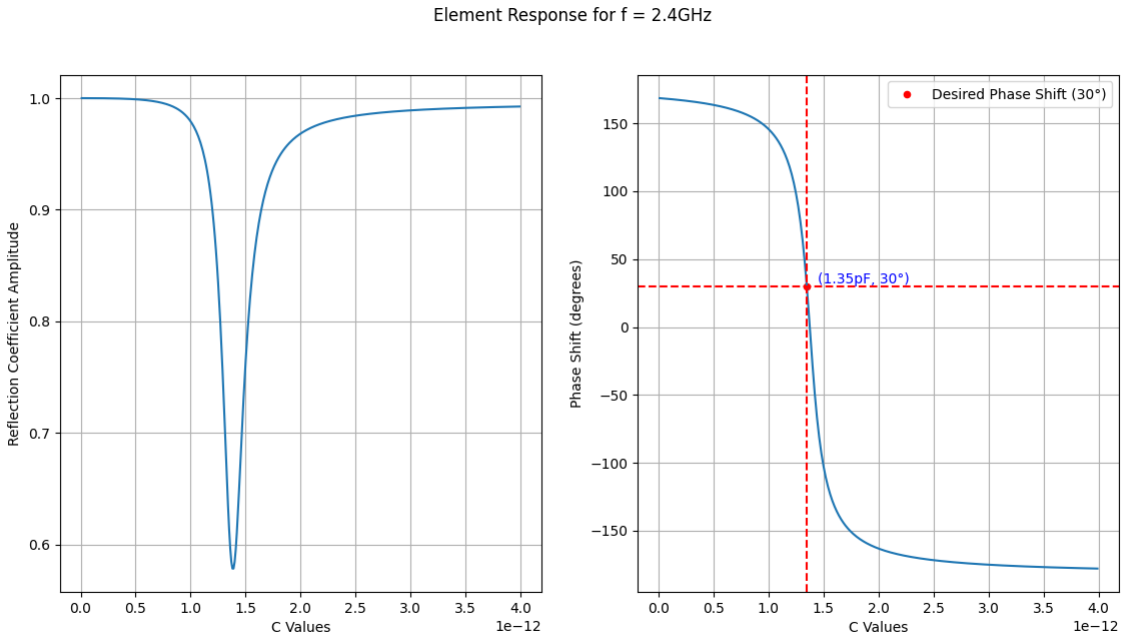

Figure 3: IRS element with varactor response (at f=2.4GHz)

Starting with varactors, A varactor diode, also known as a variable capacitance diode, is a semiconductor device designed with a p-n junction that exhibits a capacitance that can be modified through the variation of the reverse-bias voltage applied across its terminals. The capacitance property of the varactor diode is highly sensitive to changes in the voltage, leading to an adjustable capacitance that is inversely proportional to the reverse-bias voltage magnitude. Due to this feature, varactors are the main element responsible for controlling the phase shift of the element. As we will see later in details, a single element of the metasurface will be modeled as an electronic circuit having all passive circuit components. The only variable that will be able to control the reactive part of the circuit which is responsible for changing the phase is the capacitance which is decided by the value of the varactor diode based on the given bias-voltage on its terminals. The concept of leveraging varactors within Reconfigurable Intelligent Surfaces (IRS) offers both unique advantages and notable challenges. Theoretically, to attain optimal reflection control, we need to achieve a surface with a continuous and seamlessly smooth phase shift behavior. Varactor-based models strive to emulate this desired smoothness to the greatest extent possible; they are able to cover a big range of angles. In the Figure 3 above we can see the amplitudes and the angles of the reflection coefficient with different C values for a frequency $f = 2.4GHz$. We can see that the capacitances are chosen in the right range for the reflection coefficient angle to cover a range very close to the $[-180° \; 180°]$ range.

However, the practical application of varactors comes with certain complexities. Achieving accurate control over continuous capacitance poses a considerable challenge due to some complexities involved. As one ascends the frequency spectrum, the viable capacitance range diminishes substantially. Notably, at higher frequencies like around 100GHz, the required capacitance range to produce a 360-degree phase shift shrinks to femtofarad magnitudes, a range that proves challenging to accurately achieve using varactors.

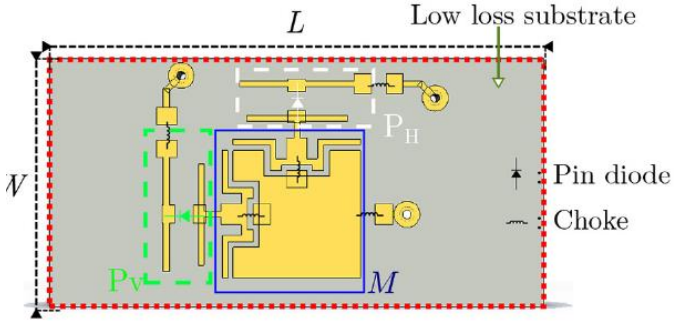

Figure 4: Model of an element with PIN diode [1]

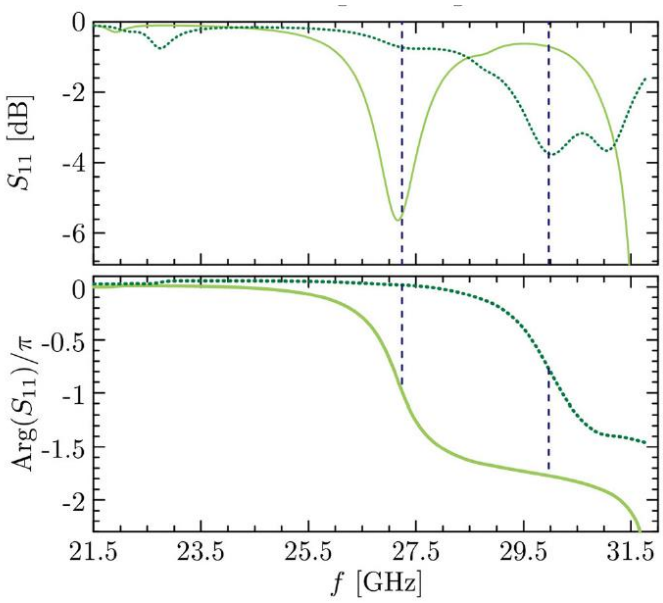

Figure 5: Response of the element with pin diode

A potential remedy to this issue lies in exploring alternative models, such as the utilization of PIN diodes, which will be explained upon in the subsequent section of this presentation. While varactors demonstrate promise in enabling responsive phase modulation, the precision demands, and limitations they face in higher frequency regimes necessitate a thorough evaluation of alternative solutions like PIN diodes for optimal performance within the context of IRS applications. It is worth noting in the end that because of the smoothness of the phase shift on the metasurface, the behavior analysis approach used with IRS using varactor diodes in the ray-optics method which present a simple yet effective analysis with and accurate results.

On the other hand, implementing surfaces with elements based on PIN diode model, this simple yet effective method will not be usable anymore. The reason is that surfaces with PIN diode elements can only produce discrete number of phase shifts depending on the number of diodes used to build each element and their states while functioning. Usually, these kinds of elements are designed to produce either two phase shifts $[0, 180]$ $degrees$ or four phase shifts $[0, 90, 180, 270]$ $degrees$. This kind of surface is good because it offers less complexity in controlling the surface phase shift and offers better compatibility with signals having very high frequencies in the ranges where surfaces with varactor elements start to fail. Another challenge while using this configuration is choosing the best combination of configuration and dimensions for all components of the element in order to have its resonating frequency equal to the frequency of the incoming signal so we can ensure the desired functionality. So, in this case do study the behavior of the surface, the only option available is the Wave-optics approach, where Maxwell's equations will be used to calculate the interactions between the scattered reflected wave of every element on the surface, where signals will interfere constructively in the receiver direction and destructively in all the other direction creating a beam directed toward the receiver.

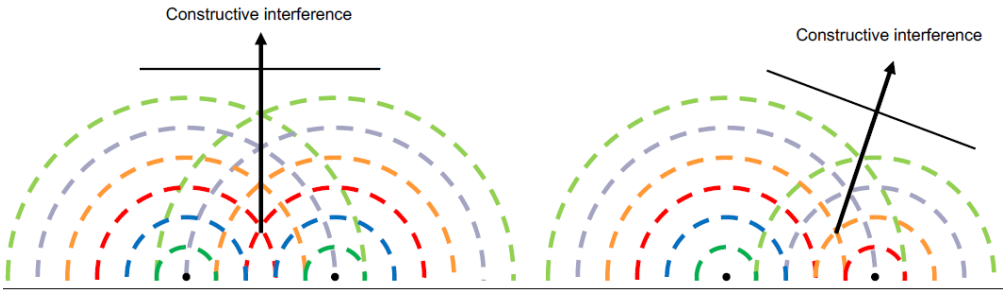

Figure 6: Visualization if the constructive interference between two elements

In fact, Gros et. al in their paper entitled: "A Reconfigurable Intelligent Surface at mmWave Based on a Binary Phase Tunable Metasurface" [1], studied this effect and came up with the series of equations explaining the control and the behavior of the surface. In their approach, the phase shift of every element of the metasurface will be calculated as follows:

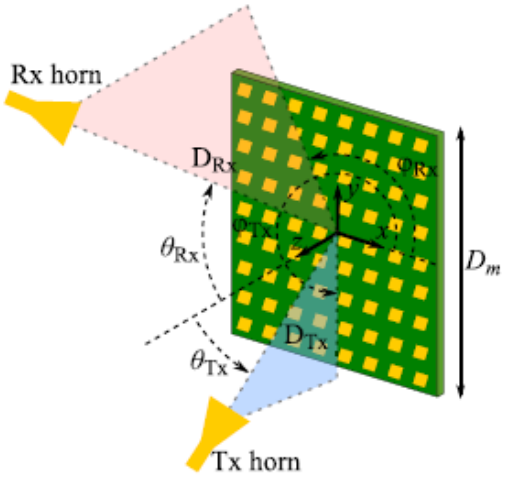

Figure 7: Angles used to calculate the phase shifts of each element [1].

- Metasurface lies in the x-y plane.
- Denoting v_T vector from the transmitter and an element of the surface
- Denoting v_R vector from the transmitter and an element of the surface
- D_{Tx} is the distance between the transmitter and an element of the surface.
- D_{Rx} is the distance between the receiver and an element of the surface.
- θ_{Tx} is the angle between the vector v_T and the normal to the surface (z-axis)
- θ_{Rx} is the angle between the vector v_R and the normal to the surface (z-axis)
- φ_{Tx} is the angle between the x axis and the projection of the vector v_T onto the x-y plane.
- φ_{Rx} is the angle between the x axis and the projection of the vector v_R onto the x-y plane.

These notations presented above in Figure 7 will be used in the following calculation.

For the Near-Field Configuration:

$$\varphi_{nm} = -k \sin(\theta_{Rx}) \left[x_n \cos(\varphi_{Rx}) + y_m \sin(\varphi_{Rx})\right] + k\sqrt{(x_n - x_{Tn})^2 + (y_n - y_{Tn})^2 + {z_{Tx}}^2} \quad (22)$$

Where:

$x_{Tx} = D_{Tx} \sin(\theta_{Tx}) \cos(\varphi_{Tx})$

$y_{Tx} = D_{Tx} \sin(\theta_{Tx}) \sin(\varphi_{Tx})$

$z_{Tx} = D_{Tx} \cos(\theta_{Rx})$

For the Far-Field Configuration:

$$\varphi_{nm} = -k \sin(\theta_{Rx}) \left[x_n \cos(\varphi_{Rx}) + y_m \sin(\varphi_{Rx})\right] + k \sin(\theta_{Tx}) \left[x_n \cos(\varphi_{Tx}) + y_m \sin(\varphi_{Tx})\right] \quad (23)$$

Then after calculating this phase shift, it will be quantized as follows:

$$\begin{cases} 0 \; if \; -\dfrac{\pi}{2} \leq \varphi_{nm} \leq \dfrac{\pi}{2} \\ \pi \; otherwise \end{cases}$$

Finally, the radiation pattern created by the IRS is formulated as follows:

$$E_r(\theta, \varphi) = \cos(\theta) \sum_{n,m=1}^{N} \Gamma_{nm} \, E_i(x_n, y_m) \, \cos(\theta_{nm}) \, e^{-\mathrm{j}\, \mathrm{k} \sin(\theta)[x_n \cos(\varphi) + y_m \sin(\varphi)]} \quad (24)$$

Where:

- $\cos(\theta)$ represents the radiation pattern of each individual element.
- Γ_{nm} is the reflection coefficient of each ech individual element.
- $E_i(x_n, y_m)$ is the electric field of the incident wave at the $nmth$ element.

5. IRS usages

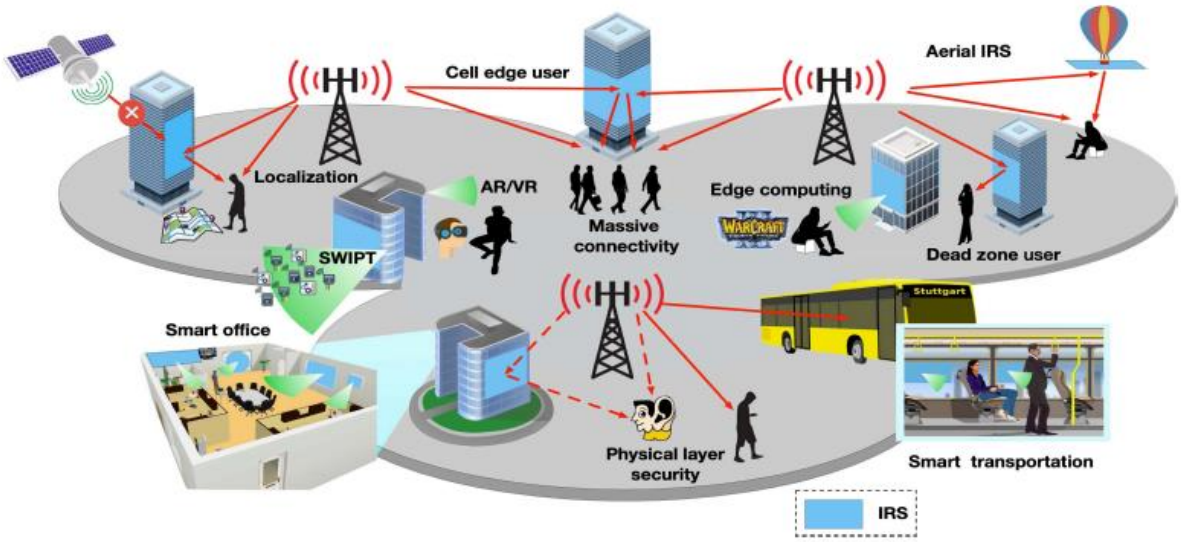

Figure 8: Illustration of IRS usages in the Future [2]

Reconfigurable Intelligent Surfaces (RISs) are emerging as a revolutionary technology, paving the way for promising future applications. In the context of smart radio environments, these surfaces demonstrate a remarkable potential to tackle a multitude of challenges. For instance, RISs can be strategically configured to bridge coverage gaps in areas with poor or no line-of-sight communication, effectively establishing adaptable non-line-of-sight links. This could significantly extend the reach of wireless networks, providing connectivity in previously inaccessible zones. Moreover, the dynamic nature of RISs allows them to serve as interference mitigators. By manipulating signal directionality, RISs can enhance signal quality and concurrently suppress unwanted signals that might otherwise cause interference with neighboring communication systems [9].

On the other hand, security, which is an essential concern in wireless communication, finds an elegant solution in the application of RIS. Functioning analogously to interference suppression, RISs can strategically manipulate signal reflections, creating destructive interference patterns or redirecting signals away from unauthorized users. This not only enhances communication privacy but also safeguards against unauthorized eavesdropping attempts [2], [9].

Beyond the security application, RISs hold immense potential to elevate the fundamental capabilities of wireless systems. By optimizing the configuration of these surfaces, wireless environments can be reshaped to augment channel rank and focus radio waves. This facilitates higher data rates and precision in location-based services [9].

RISs further exhibit strength in information and power transfer scenarios. These surfaces can concentrate energy towards specific sensor nodes, paving the way for simultaneous energy replenishment and data transmission. Additionally, the concept of ambient backscattering is harnessed, where RISs enable low-power sensors to encode data into existing radio waves, thus repurposing ambient signals for communication [2], [9].

The versatility of RIS applications spans numerous settings, from smart cities and homes to transportation hubs and more. Notably, the integration of RISs in such environments not only enhances coverage and connectivity, but also does it in a way that is discreet and visually pleasing. Moreover, RISs become the solution of choice for situations where traditional base stations are unsuitable, such as in densely built urban areas or high-security zones. This transformative potential of RISs in Smart Radio Environments (SREs) marks a paradigm shift in wireless communication strategies, offering innovative solutions to connectivity challenges and resource optimization [9].

UAV Communications emerges as a novel frontier with the introduction of aerial IRS (AIRS). By mounting IRSs on unmanned aerial vehicles (UAVs), AIRS expands service regions and enables full-range reflection, effectively addressing blockage and enhancing line-of-sight connections. The unique advantage of AIRS lies in its ability to establish 360-degree panoramic full-range reflection, facilitating communication between any pair of ground nodes within its coverage area. However, the dynamic nature of UAV movement introduces complexities in channel estimation and tracking, necessitating novel methods to maintain efficient communication links [2].

In the context of millimeter-wave (mmWave) communications, RISs prove invaluable in mitigating signal blockage and high propagation loss through the creation of virtual Line-of-Sight (LoS) channels. Furthermore, the integration of RISs in mobile edge computing (MEC) systems presents opportunities for optimized computation offloading and resource allocation, yielding reduced latency and energy efficiency gains.

The extensive landscape of RIS applications extends to cognitive radio networks, full-duplex communication, sensing, localization, and even terahertz communications. These diverse areas underscore the transformative capabilities and research potential that RISs offer to wireless communication systems [2]. In essence, reconfigurable intelligent surfaces emerge as a versatile toolkit with the capacity to reshape wireless communication paradigms and surmount multifaceted challenges across a variety of applications [2], [9].

Smart Radio Environments (SREs) offer diverse scenarios where Reconfigurable Intelligent Surfaces (RISs) can redefine wireless communication. RISs on large buildings enhance coverage in smart cities. Homes benefit from RIS-coated walls, boosting local device connectivity. Smart buildings utilize RISs on windows for improved indoor-outdoor links. Harsh environments in factories are transformed by RIS reflections. Hospitals use RISs to expand coverage while reducing EM exposure. RIS-coated campuses eliminate the need for multiple access points. Complex undergrounds achieve connectivity via RIS deployment. Train stations employ RISs for better signals. Airports enhance hallways with RIS-directed beams. Smart billboards, glasses, clothing, cars, trains, and airplanes all leverage RISs. Aesthetically, RISs blend seamlessly while enhancing wireless connectivity. In conclusion, RISs unlock SRE potential, adapting to diverse settings and resolving wireless challenges [9].

D. A digital twin for intelligent surfaces aided cellular network infrastructures - CONVERGE Project

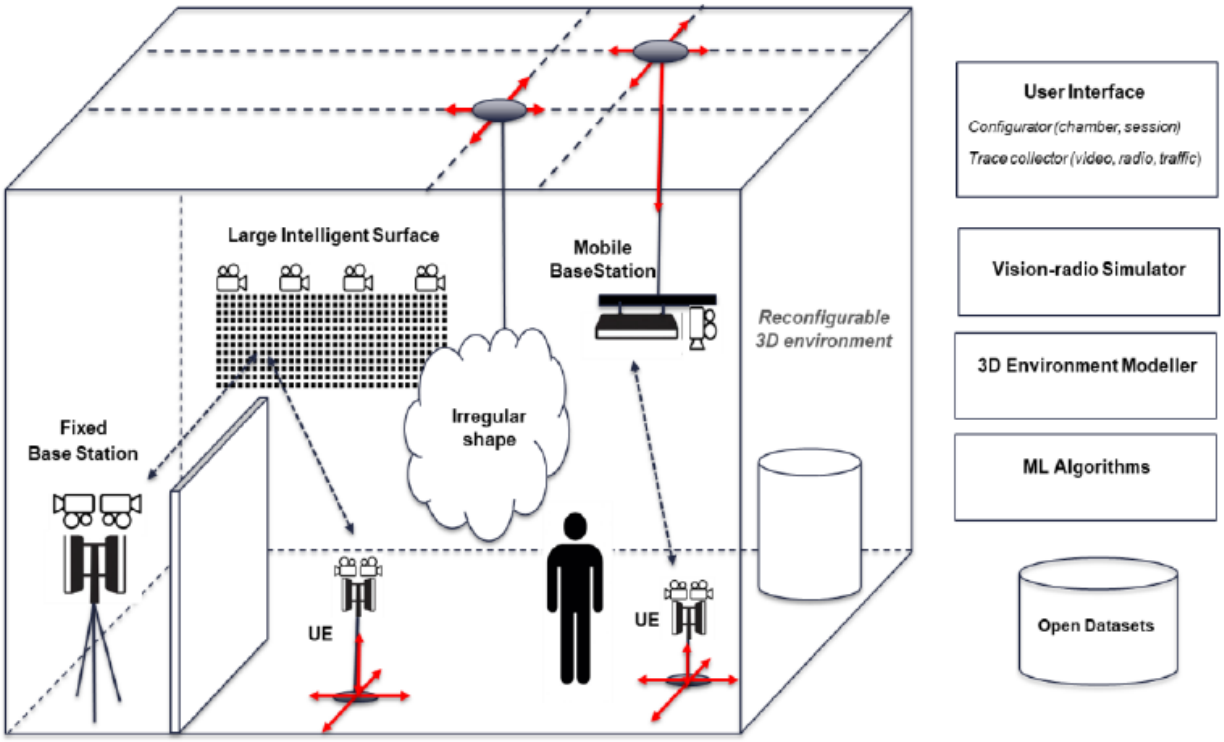

Figure 9: Concept of the proposed vision-radio experimental chamber [14]

Before digging deeper into the IRS concept, we need first to understand the purpose behind working on this project. IRS simulation and deployment is part of a European project called CONVERGE. The main objective of the CONVERGE project is the development of an innovative toolset combining radio and vision-based communications and sensing technologies to enable an emerging area of research aligned with the motto “view-to-communicate and communicate-to-view”. This toolset will be deployed in an anechoic experimental chamber that will be called vision-radio experimental chamber. It will have the configuration shown in Figure 9 above. Here we have a 3D-digital twin of a real physical environment used to validate the proof-of-concept results of experiments and calibrate the simulator environment to understand the level of accuracy needed from geometric and electromagnetic models to obtain the required performance and efficiency. INRIA’s task is to design and simulate the IRS in order to control radio waves in this wireless environment.

Notably, the experimental chamber offers remote controllability to researchers via a user interface, facilitating precise manipulation of factors such as object positioning, mobility patterns, traffic generation dynamics, as well as reflective and sensing strategies. The heart of the toolset resides in the visionary-radio simulator, ingeniously harnessing a 3D environment modeler to facilitate the instantiation of the digital twin of the visionary-radio chamber by leveraging information from both vision and radio sensors.

The signal propagation simulator employs the carefully constructed 3D models generated by the environment modeler to accurately simulate radio propagation conditions. Among the relevant components of this comprehensive toolset is a vision-enabled intelligent surface, equipped with both passive and active operational modes. In its passive mode, this surface enables controlled reflection of radio waves originating from base stations and user equipment. By integrating machine vision through strategically positioned cameras, the intelligent surface acquires the ability to perceive its surroundings. Upon activation of its active mode, the surface seamlessly transforms into a base station, forming intricate beams, orchestrating traffic scheduling, and effectuating traffic exchange. A pivotal feature is its capacity to gather insights from the environment using radio frequency waves—operating through the deliberate emission of controlled, directive radio waveforms and subsequent reception of echoes. This unique capability empowers the intelligent surface to generate RF-based videos that clearly describe the examined environment via computational imaging, which can be seamlessly combined with videos captured by the integrated cameras. Crucially, the versatility of this toolset extends its applicability beyond the visionary-radio experimental chamber, permeating diverse research infrastructures including manufacturing facilities, warehouses, hospitals, as well as dynamic media scenarios such as music festivals and exhilarating sporting events. This ambitious effort stands as a demonstration of the project's commitment of pushing the boundaries of innovation, seamlessly fusing vision, communication, and sensing technologies to forge new horizons in research and application.

E. IRS Model Simulator Design

Having outlined the current state of research in the field of intelligent reconfigurable surfaces, along with its significance, applications, and operational principles, we shall now transition to the subsequent section of this report. In the forthcoming segment, we will introduce the design of our IRS simulator model.

We consider that we have a fixed coordinates system (x, y, z) defined by the location of the metasurface. This surface will be lying in the x-y plane of our coordinates system. The first element of this metasurface (upper left element) will be located at point (0, 0, 0) the origin of our coordinate system. The width of the surface will be spanning along the x direction, and the height will go along the y direction.
The z-axis will be the axis perpendicular to the surface, so the normal vector to the surface will be the unit vector $u_z = [0, 0, 1]$ along the z-axis.

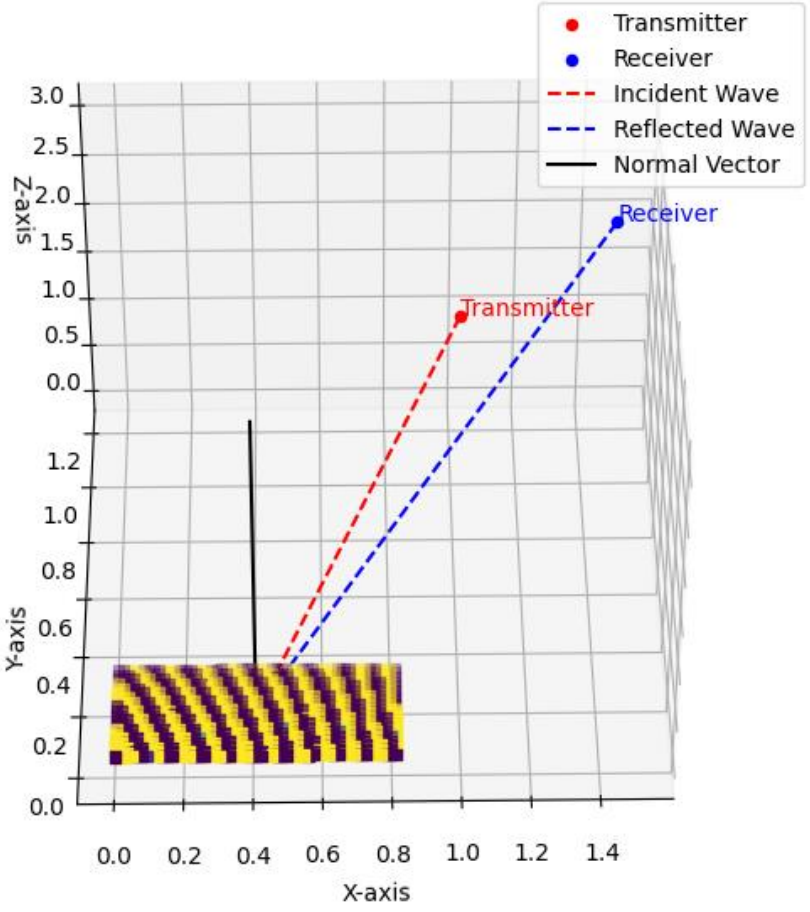

Figure 10: Metasurface model

We start by giving the following inputs to the model:

- Transmitter coordinates: $t_x = [x_i, y_i, z_i]$
- Receiver coordinates: $r_x = [x_r, y_r, z_r]$
- Index of refraction of free space n_i

- For the transmitted signal:
  - Transmitted Signal Frequency $f\ (in\ Hz)$
  - Transmitted Signal Amplitude $A_i\ (in\ V)$
  - Transmitted Signal Phase $\varphi_i\ (in\ rad)$

- For the varactor:
  - Element Resistance value $R\ (in\ \Omega)$
  - Element bottom layer inductance $L_1\ (in\ H)$
  - Element top layer inductance $L_2\ (in\ H)$
  - Element effective capacitance $C\ (in\ F)$
  - Capacitance range that the varactor can produce.

- For the metasurface:
  - Surface dimensions (w_x, h_y)
    Where w_x is the number of elements along the width of the surface (in the x direction)
    h_y is the number of elements along the height of the surface (in the y direction)
  - Elements size $e\ (in\ m)$
    Where the elements are considered as square with edge length e.
  - Element spacing $\Delta_e\ (in\ m)$
    Where element spacing Δ_e is the spacing between the edge of the first element and the edge of the second element.
    Element spacing is the same in both x and y directions.

Then using the inputs, we previously mentioned, we can calculate some parameters as follows:

- Wavelength $\lambda = \frac{c}{f}\ (in\ m)$
  Where $c = 3 \times 10^8\ (in\ m/s)$ is the speed of light.
- $Angular\ frequency\ \omega = 2\pi f\ (in\ rad/s)$
- $Wave\ number\ k_0 = \frac{2\pi}{\lambda}$
- The distance between the middle of 2 consecutive elements of the surface in both x and y directions: $\Delta = e + \Delta_e\ (in\ m)$

The aim of this work is to design a better Reconfigurable intelligent surface that can be reprogramed instantaneously in order to reflect an input signal from a given transmitter toward a known receiver.
The main working principle of this surface will follow the generalized Snell's law for anomalous reflection in 3D space. This law is modeled by the following equations:

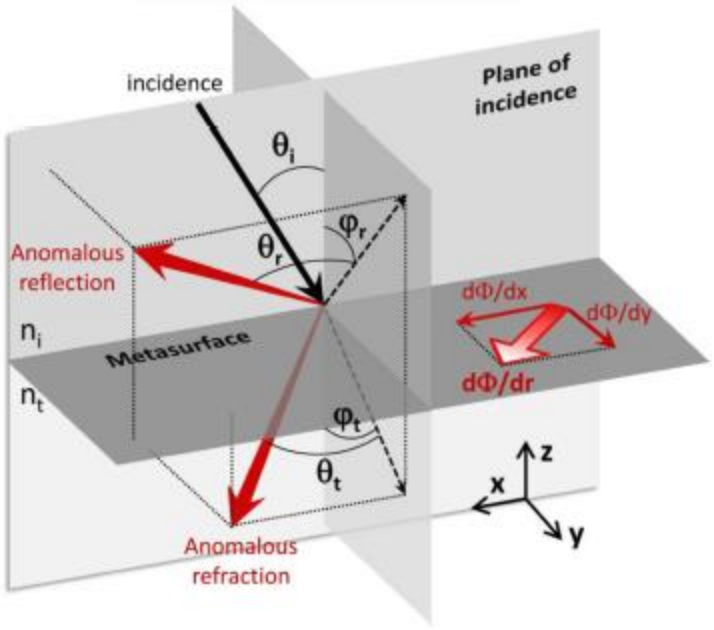

Figure 11: figure showing the angles used in the generalized Snell's law equations.

$$\sin(\theta_r) - \sin(\theta_i) = \frac{1}{n_i k_0}\frac{\partial\phi(x,y)}{\partial x} \tag{25}$$

$$cos(\theta_r)\, sin(\varphi_r) = \frac{1}{n_i k_0}\frac{\partial\phi(x,y)}{\partial y} \tag{26}$$

We denote by $v_{r,proj}$ the projection of the reflected vector v_r onto the plane perpendicular to the incident plane of incidence.
φ_r is the angle between the vector $v_{r,proj}$ projection of the reflected vector and the z-axis.
θ_r is the angle between the reflected vector v_r and its projection vector $v_{r,proj}$
n_i is the Index of refraction of free space.
$k_0 = \frac{2\pi}{\lambda}$ is the wavenumber.
$\phi(x,y)$ is the phase shift introduced by each element on the surface; $\frac{\partial\phi(x,y)}{\partial x}$ and $\frac{\partial\phi(x,y)}{\partial y}$ are the gradients of the phase shifts going in x and y direction respectively.

We know the location of the transmitter and the receiver, and we want to properly reflect the signal toward the receiver.
Based on this information, we can geometrically calculate the values of the reflection angles θ_r and φ_r to be able to calculate later the phase shifts needed for every element.
We consider that the transmitter is equipped with an omnidirectional antenna radiating in all directions. In our model we will discretize the propagation sphere by modeling it using equidistant rays generated from the transmitter and hitting each element of our surface. So, our model will only consider the part of the transmission sphere that will reach our surface, and it will be modeled as a ray hitting each element of our surface. So, the number of considered rays is equal to the number of elements on the surface. These rays will be represented by a (w_x, h_y) matrix each entry of this matrix contain $v_i = [x_i, y_i, z_i]$ the

coordinates of the incident ray hitting the corresponding element. These vectors will be calculated geometrically for every element using the following formula:

$$v_i = element[x, y, z] - t_x \tag{27}$$

Since our goal is to reach the receiver with all the reflected rays, we will calculate the theoretical reflected rays considering all of them will reach the receiver. These rays will be represented by a (w_x, h_y) matrix each entry of this matrix contain $v_r = [x_r, y_r, z_r]$ the coordinates of the reflected ray hitting the receiver. These vectors will be calculated geometrically for every element using the following formula:

$$v_r = r_x - element[x, y, z] \tag{28}$$

After calculating the incident and the reflected vectors, the next step is to calculate the incident and the reflection angles. These angles are θ_i, θ_r and φ_r shown in the Figure 11 above.
θ_i is the angle between the incident vector v_i and the normal to the plane which is in our case unit vector $u_z = [0, 0, 1]$ along the z-axis.
θ_r and φ_r are the angles between the reflected vector v_r and $v_{r,proj}$, and $v_{r,proj}$ and u_z respectively. We remind you that $v_{r,proj}$ is the projection of the reflected vector v_r onto the plane perpendicular to the incident plane of incidence. Details about the of $v_{r,proj}$ are found in the Appendix 1 at the end of this document.
After successfully calculating the angles θ_i, θ_r and φ_r geometrically, now we can calculate the gradient phase shifts needed to reflect the transmitted signal toward the receiver location. To compute the phase shift gradient in both x and y direction we will use the generalized Snell's law that we presented previously in equations (25) and (26).

$$\frac{\partial \phi}{\partial x}(x, y) = n_i k_0 (\sin(\theta_r) - \sin(\theta_i)) \tag{29}$$

$$\frac{\partial \phi}{\partial y}(x, y) = n_i k_0 \cos(\theta_r) \sin(\varphi_r) \tag{30}$$

After this step we will have 2 (w_x, h_y) matrices first the phase shift gradient along x direction, the second is the phase shift gradient along the y direction.
The next step is to use the $\frac{\partial \phi}{\partial x}(x, y)$ and the $\frac{\partial \phi}{\partial y}(x, y)$ matrices to find the phase shift $\phi(x, y)$ for every element of the surface. Because theoretically we should only have one phase shift $\phi(x, y)$ based on its x and y calculated previously, $\phi(x, y)$ will be calculated separately using $\frac{\partial \phi}{\partial x}(x, y)$ and $\frac{\partial \phi}{\partial y}(x, y)$ and then averaging out both results to get one final phase shift.

$$\phi(x, y) = \frac{\phi_x(x, y) + \phi_y(x, y)}{2} \tag{31}$$

This function represents the phase shift that each element should apply on the incoming signal in order to have the desired reflection. $\phi(x, y)$ will be a 2D matrix of size (w_x, h_y), where each entry represents the phase shift required to be produced by the corresponding element of the metasurface.
Calculation details can also be found in the Appendix 2 at the end of this document.
The Figure 12 below shows the theoretical phase shift required by every element in order to obtain a reflection in the designated receiver direction.

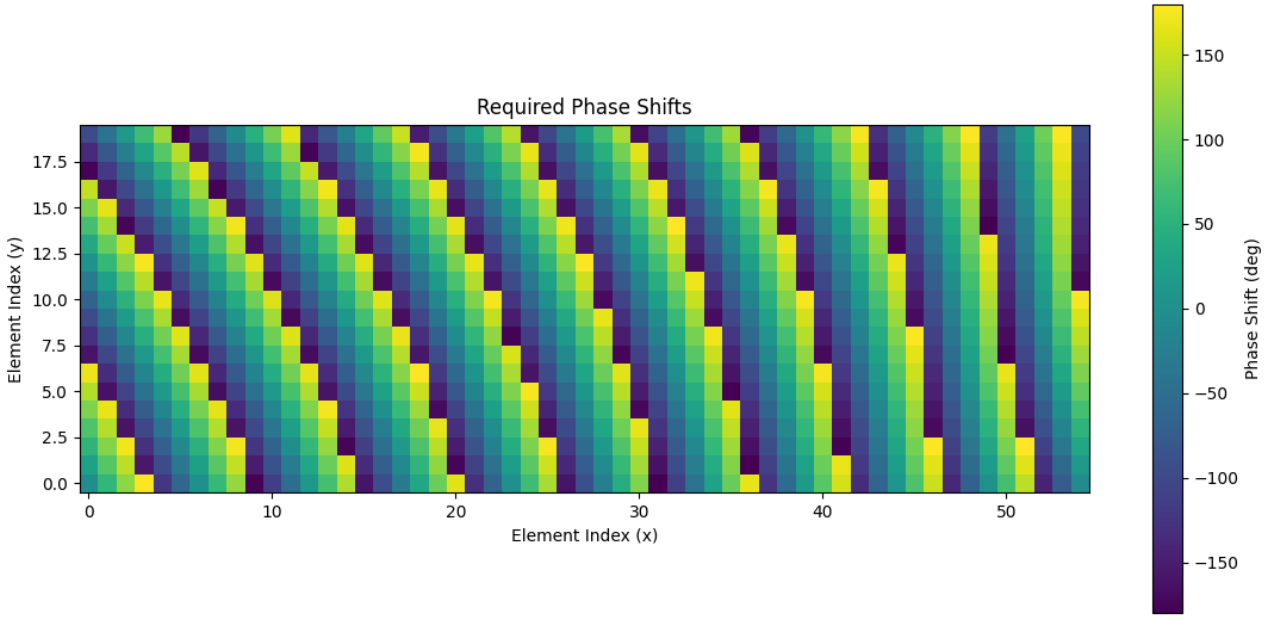

Figure 12: Required phase shifts.

Now that we have calculated the phase shift required by every element of the surface, we should procced in calculating the required capacitance for the element to produce this phase shift, and ultimately calculate the bias voltage that should be supplied to the varactor in order the produce the required capacitance.
We can find the phase shift of an element by checking its reflection coefficient Γ calculated using equation (10).
Knowing that the following model is using RIS with varactors to control the phases of the elements.
Below we will see the reflecting element electronic model and we will calculate Z_n.

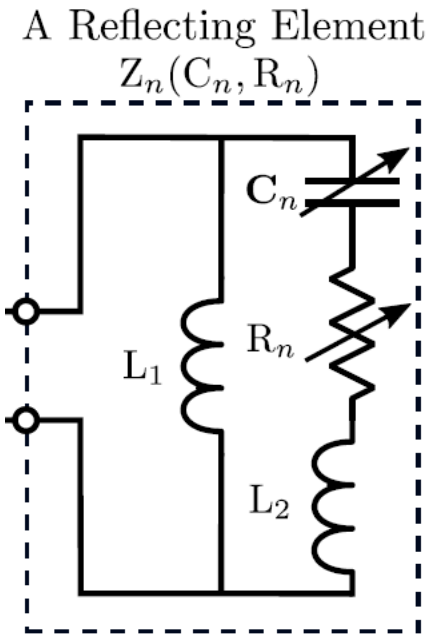

Figure 13: reflecting Element electronic model

We can see in Figure 13 the electronic model for a reflecting element. The impedance of this element can be calculated as follows:

$$Z_n = \frac{j\omega L_1 \left(j\omega L_2 + \frac{1}{j\omega C_n} + R_n\right)}{j\omega L_1 + \left(j\omega L_2 + \frac{1}{j\omega C_n} + R_n\right)} \tag{32}$$

Where:

- R_n: effective resistance of element
- L_1: bottom layer inductance of the element
- L_2: top layer inductance of the element
- C_n: effective capacitance of an element
- ω: angular frequency ($\omega = 2\pi f$)

R_n, L_1, L_2, are fixed values representing the physical characteristics of the element, ω will also be known dependent on the frequency of the impinging signal. the only variable is the tunable capacitance C_n of the elements.

Then to calculate the required capacitance value that will create the desired phase shift, we have to guess a C_n value that will give the element a certain impedance Z_n and plugging this Z_n in the reflection coefficient equation Γ we should have the angle equal to the desired phase shift. The range of C_n values is decided by the model of the varactor used in the element and the capacitance range that it able to produce when given different voltages. This varactor should be sized to correspond to the predicted frequencies that will be used on this surface. In other words, the capacitance range that this varactor should produce should be in the exact range to be able to cover all the angles between $[-180°\ 180°]$.

In what follows I will describe the strategy used to estimate the capacitance needed to create the desired phase shift:

1. First, as we spoke earlier, we will identify the range of that capacitance C_n available. We should create a 1D matrix containing these capacitance values.
2. Using the available capacitance matrix, we will calculate the element impedance Z_n that could be created for each value of C_n. (Knowing that the values of R_n, L_1, L_2 are constants).
   Then the result will be an array of impedances having the same length as the array of available capacitances, and the value of the impedance on a given location of the array will corresponds to the value of the capacitance form the available capacitances array in the same location.
3. Using the achievable element impedances calculated earlier, we will now calculate the reflection coefficient Γ of the element that could be achieved by the given element impedances.
   The result will also be an array of reflection coefficients having the same length as the array of available capacitances, and the value of the reflection coefficient on a given location of the array will corresponds to the value of the capacitance form the available capacitances array in the same location.
4. In this step we will calculate the angles of every reflection coefficient we have in the elements achievable reflection coefficients array calculated in the previous step.
   The result will also be an array of reflection coefficients angles having the same length as the array of available capacitances, and the value of the reflection coefficient angle on a given location of the array will corresponds to the value of the capacitance form the available capacitances array in the same location.
5. Now we have a connection between the capacitance and the phase shifts angles (which is basically the reflection coefficients angles array). The last thing left to do is to estimate the value of the capacitance C for a given phase shift. This estimation will be done by interpolation.
   (Note: the more capacitance values we have in the initial available capacitance matrix, the more accurate the estimated capacitance will be at the end of this method)

So finally, we take the phase shifts matrix $\phi(x, y)$ that we calculated previously and apply the capacitance estimation method that we discussed earlier to find in the end the required capacitance for every element to achieve the desired phase shift. The result after this method will be a 2D matrix of size (w_x, h_y), where each entry represents the required capacitance to be tuned in the corresponding element of the metasurface to achieve its desired phase shift $\phi(x, y)$.

In the next step, we will calculate the real phase shift that will be actually produced by the surface based on the estimated capacitance value we calculated in the previous step. The importance of this step lies in the fact that due to the complexity of the problem, the capacitance C_n is not calculated exacly, instead it was estimated based on the phase shift needed. Also, the element should be able to produce the estimated capacitance exacly, which could be hard sometimes and it could lead to some difference between the calculated and the real phase shift. Therefore, to take this into account, the real phase shift will be calculated as follows:

1. Using the estimated elements capacitance matrix calculated earlier, we will calculate the real element impedance Z_n using its equation that we provided earlier. (Knowing that the values of R_n, L_1, L_2 are constants).

Then the result will be a 2D matrix of size (w_x, h_y), where each entry represents the actual impedance of the corresponding element on the metasurface.

2. Using the elements impedances calculated earlier, we will now calculate the reflection coefficient Γ of the elements given their impedances.
   Then the result will be a 2D matrix of size (w_x, h_y), where each entry represents the actual reflection coefficient of the corresponding element on the metasurface.
3. Now to find the real phase shifts, all what is left to do is to calculate the angle of each reflection coefficient in the real reflection coefficient matrix.
   Then the result will be a 2D matrix of size (w_x, h_y), where each entry represents the real phase shifts $\phi_{real}(x, y)$ that will be introduced by the corresponding element on the metasurface.

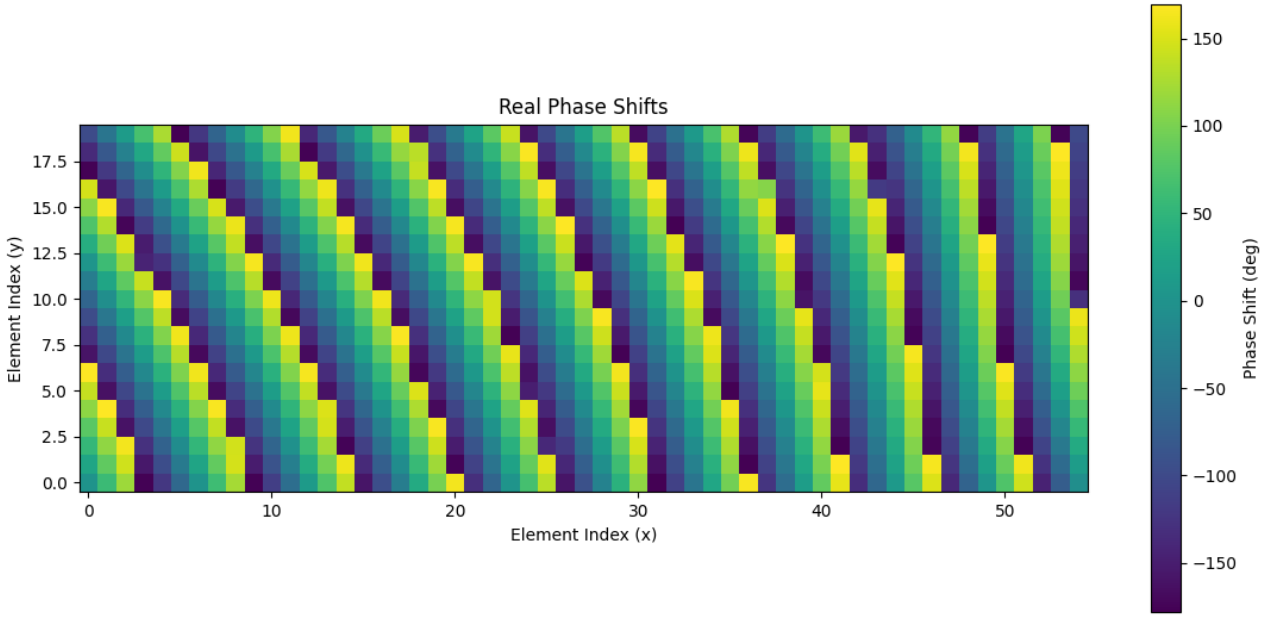

Figure 14: Real Phase shifts

Then from the calculated real phase shifts of each element we can calculate the real reflection angles θ_r and φ_r of the reflected signal. To do so, we will derive $\phi_{real}(x, y)$ in both x and y directions to get the gradient of the real phase shift used in the generalized Snell's law equations (25), (26).

To derive real phase shifts $\phi_{real}(x, y)$ we will be using the following derivation formulas, considering the fact that the phase shifts should always be in the $[-\pi\ \pi]$ range, so even when subtracting 2 values of the $\phi_{real}(x, y)$, we should make sure that it belongs to the range $[-\pi\ \pi]$.

As an example:

$[\phi_{real}(x+1,y)-\phi_{real}(x,y)]mod[-\pi\ \pi]$

This equation means that the resultant of $\phi_{real}(x+1,y)-\phi_{real}(x,y)$ will be moved to the $[-\pi\ \pi]$ range.

Taking all of the above into account we will have the following equations to perform the derivatives:

In the x direction $\frac{\partial\phi_{real}}{\partial x}(x,y)$:

$First\ column\ (x=0)\colon \frac{\partial\phi_{real}}{\partial x}(x,y)=\frac{[\phi_{real}(x+1,y)-\phi_{real}(x,y)]mod[-\pi\ \pi]}{\Delta x}$

$Last\ column\ (x=-1)\colon \frac{\partial\phi_{real}}{\partial x}(x,y)=\frac{[\phi_{real}(x,y)-\phi_{real}(x-1,y)]mod[-\pi\ \pi]}{\Delta x}$

$Middle\ columns\ (x=[1,\dots,-2])\colon \frac{\partial\phi_{real}}{\partial x}(x,y)=\frac{[\phi_{real}(x+1,y)-\phi_{real}(x-1,y)]mod[-\pi\ \pi]}{2\times\Delta x}$

In the y direction $\frac{\partial\phi_{real}}{\partial y}(x,y)$:

$First\ column\ (y=0)\colon \frac{\partial\phi_{real}}{\partial y}(x,y)=\frac{[\phi_{real}(x,y+1)-\phi_{real}(x,y)]mod[-\pi\ \pi]}{\Delta y}$

$Last\ column\ (y=-1)\colon \frac{\partial\phi_{real}}{\partial y}(x,y)=\frac{[\phi_{real}(x,y)-\phi_{real}(x,y-1)]mod[-\pi\ \pi]}{\Delta y}$

$Middle\ columns\ (y=[1,\dots,-2])\colon \frac{\partial\phi_{real}}{\partial y}(x,y)=\frac{[\phi_{real}(x,y+1)-\phi_{real}(x,y-1)]mod[-\pi\ \pi]}{2\times\Delta y}$

Then after successfully finding the gradients of the real phase shifts $\phi_{real}(x,y)$, $\frac{\partial\phi_{real}}{\partial x}$ and $\frac{\partial\phi_{real}}{\partial y}$. We can now use them to calculate the real reflected angles θ_r and φ_r based on the generalized Snell's law of reflection. Then:

$$\theta_r=\sin^{-1}\left(\frac{1}{n_i k_0}\frac{\partial\phi(x,y)}{\partial x}+\sin(\theta_i)\right) \tag{33}$$

$$\varphi_r=\sin^{-1}\frac{1}{n_i k_0\cos(\theta_r)}\frac{\partial\phi(x,y)}{\partial y} \tag{34}$$

The results after this method will be two 2D matrix of size (w_x,h_y) each, the first is the angle θ_r of the reflected ray from each element. The second is the angle φ_r of the reflected ray from each element.

By finding the real reflection angles θ_r and φ_r, and knowing the location of the transmitter, the location of the receiver and the location of every element of the metasurface, we can now calculate the real reflected vector. Then after calculating the reflected vector, we will check if it hits the antenna of the receiver successfully by checking if the endpoint of the reflected vector (point $p_r(x_{pr},y_{pr},z_{pr})$) is inside

the receiver antenna defined by its shape, its dimensions and its center which is the coordinates of the receiver that we defined in the beginning. The complete calculation of the real reflected vector v_r and its extremity point p_r can be found in the Appendix 3 at the end of this document.

The next and the final step is to check if the reflected ray hits the receiver successfully. To do so we can simply define the receiver antenna shape, dimensions, and center point, then we can check it the point p_r calculated earlier, is inside or outside the area occupied by the antenna.

In the end, the result here will be a 2D Boolean "successful reflections (SR)" matrix of size (w_x, h_y), where each entry will have a Boolean "True" value indicating that the reflected ray by the corresponding element is received corrected by the receiver antenna, or a Boolean "False" value indicating that the reflected ray by corresponding element misses the receiver antenna.

After determining the reflection model, by calculating the reflection angles that will dictate the path of the ray. We can now know if a given reflected ray will reach the receiver or not. The next step is to create the power model by calculating the effective power received by the receiver antenna.
The power model to be used in our case is similar to the 2-ray model, where we calculate the power received by a receiver coming from 2 paths, one line of sight path and another non-line of sight path where the signal is reflected by a surface and the reflected ray reaches the receiver. The 2-ray power model is the following:

$$P_r = P_t \left(\frac{\lambda}{4\pi}\right)^2 \times \left| \frac{\sqrt{G_{los}} \times e^{-j2\pi l/\lambda}}{l} + \Gamma(\theta) \sqrt{G_{surface}} \frac{e^{-j2\pi(x+x')n_i/\lambda}}{x+x'} \right|^2 \quad (35)$$

$where$:
P_r: $The\ power\ received$
P_t: $The\ power\ transmitted$
$P_t = \frac{{A_i}^2}{2}, A_i\ is\ the\ amplitude\ of\ the\ transmitted\ signal$
G_{los}: $The\ gain\ of\ the\ antenna$
$G_{surface}$: $The\ gain\ of\ ths\ surface\ of\ reflection$
Γ: The reflection coefficient of the surface
l: $The\ line\ of\ sight\ distance\ between\ the\ transmitter\ and\ the\ receiver$
$(x + x')$: $The\ non\ line\ of\ sight\ distance\ between\ the\ transmitter\ and\ the\ receiver$
n_i: $The\ index\ of\ reflection\ of\ freespace$

Our study is simply considering the non-line-of-sight scenarios where the received signal will only come from the reflected part of the transmitted signal by the metasurface, without the loss of generality. In this case, we will have the line-of-sight distance ($l = +\infty$). Adapting the power equation, we get:

$$P_r = P_t G_t \left(\frac{\lambda}{4\pi}\right)^2 \times \sum_{n=1}^{N} \left(\Gamma_n \sqrt{G_{surface}} \frac{e^{-j2\pi(x_n+x'_n)n_i/\lambda}}{x_n + x'_n} \right)^2 \quad (36)$$

$Where$:

$N\ is\ the\ number\ of\ elements\ on\ the\ metasurface$
$x_n\ is\ the\ distance\ from\ the\ transmitter\ to\ the\ n^{th}\ element\ of\ the\ metasurface$
$x'_n\ is\ the\ distance\ from\ the\ distance\ form\ the\ n^{th}\ element\ to\ the\ receiver$
$(x_n + x'_n)\ is\ the\ non\ line\ of\ sight\ distance\ between\ the\ transmitter\ and\ the\ receiver$
$through\ the\ n^{th}\ element\ of\ the\ metasurface$
$\Gamma_n\ is\ the\ reflection\ coefficient\ of\ the\ n^{th}\ element\ of\ the\ metasurface$

In the equation above, we are summing over the powers of all reflected rays reaching the receiver.

The only missing thing from this equation is the fact that we have to disregard the power coming from the rays that will be reflected in an incorrect way and will not reach the receiver antenna. To take this issue into account, we will add the successful reflections (SR) matrix that we calculated previously. The power model will become:

$$P_r = P_t G_t \left(\frac{\lambda}{4\pi}\right)^2 \times \sum_{n=1}^{N} \left(SR_n \Gamma_n \sqrt{G_{surface}} \frac{e^{-j2\pi(x_n + x'_n)n_i/\lambda}}{x_n + x'_n} \right)^2 \quad (37)$$

$Where$:

$SR_n\ is\ an\ indice\ representing\ if\ the\ ray\ reflected\ by\ the\ n^{th}\ element\ of\ the\ metasurface$
$will\ reach\ the\ receiver\ antenna\ successfully$

When the reflected ray by the nth element hits the receiver successfully, $SR_n = "True"\ or\ "1"$ so we include the power of this ray when calculating the received power. But when the reflected ray by the nth element misses the receiver successfully, $SR_n = "False"\ or\ "0"$ so we multiply the power of this ray by "0" to ignore it and not take it into account when calculating the total power at the receiver.

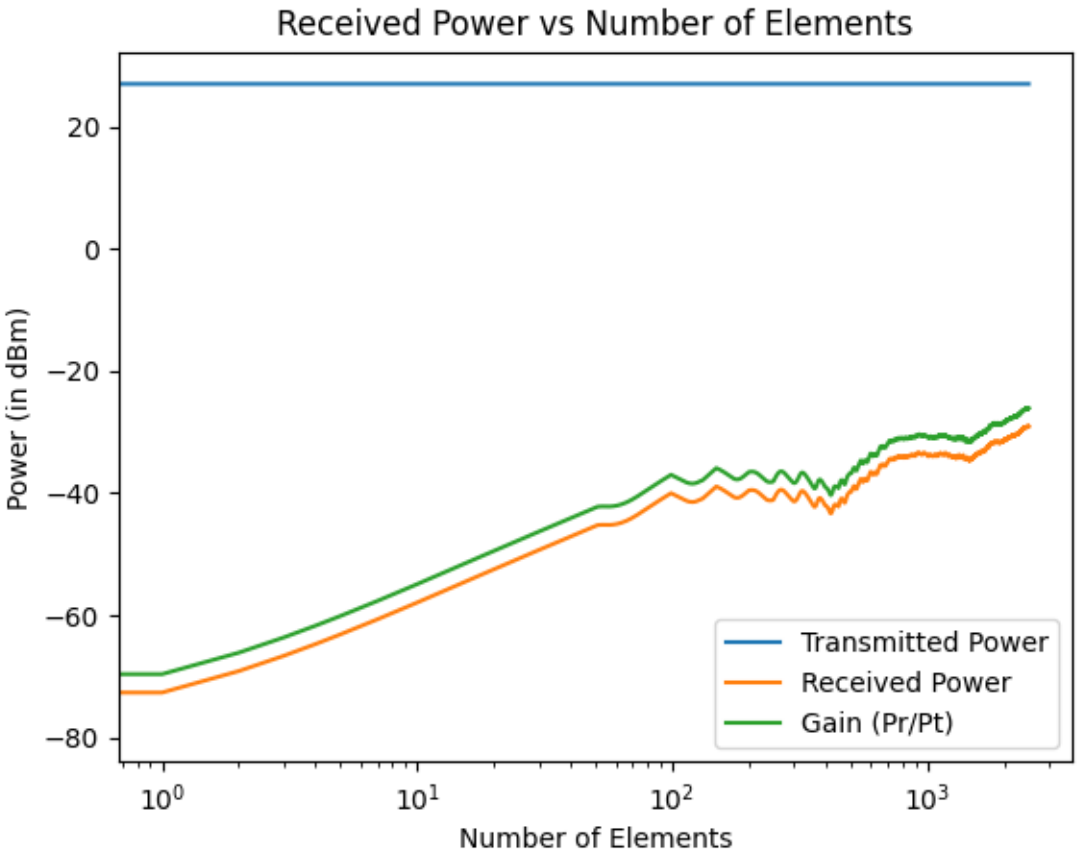

Figure 15: Power received vs number of elements.

Finally, by calculating the reflection model and the power model, we have completed the design of the Intelligent Reconfigurable Surface model. Now we have the power of the signal received. In the next part, we will calculate the power received by the receiver antenna when we do not have an intelligent metasurface and compare it with the IRS case to check the additional gain that the metasurface introduces. In this case the reflection will be governed by the original Snell's law $\theta_r = \theta_i$ and the transmitted and the reflected rays will be in the same plane, so we have $\varphi_r = 0$. Detailed calculation can be found at the end of the document in Appendix 4.

The final part is to calculate the power received by the receiver antenna in a system without a metasurface, and we do not have a line-of-sight between the transmitter and the receiver. In this case the power will be:

$$P_r = P_t G_t \left(\frac{\lambda}{4\pi}\right)^2 \times \left(\Gamma \sqrt{G_{surface}} \frac{e^{-j2\pi(x+x')n_i/\lambda}}{x+x'}\right)^2 \tag{38}$$

Where Γ is the reflection coefficient of the surface, this reflection coefficient will depend on the material of the surface, and it will be different for signals with perpendicular or parallel polarizations.

$$\Gamma_{\perp} = \frac{\cos\theta_i - \sqrt{\varepsilon_r - \sin^2\theta_i}}{\cos\theta_i + \sqrt{\varepsilon_r - \sin^2\theta_i}} \tag{39}$$

$$\Gamma_{\parallel} = \frac{(\varepsilon_r \times \cos\theta_i) - \sqrt{\varepsilon_r - \sin^2\theta_i}}{(\varepsilon_r \times \cos\theta_i) + \sqrt{\varepsilon_r - \sin^2\theta_i}} \tag{40}$$

$where$

ε_r $is\ the\ permittivity\ of\ the\ material\ composing\ the\ surface\ on\ which\ the\ signal\ will\ reflect\ back$
θ_i $is\ angle\ of\ incidence\ of\ the\ signal\ into\ the\ surface\ calculated\ in\ the\ previous\ section$
$section\ using\ the\ original\ Snell's\ law\ (\theta_i = \theta_r)$

The result of this function will be the power of the signal received by the receiver antenna in the system without Intelligent Reconfigurable Surface.

1. Results

In the final table below, we can see the results produced by our model:

Result	Value
Transmitter Location	[-1.73, 0.15, 3.0]
Receiver Location	[2.27, 0.15, 3.0]
Incident Signal frequency	10.0 GHz
Incident Signal Wavelength	29.979 mm
Surface Number of Elements	(20, 55)
Surface Elements Sizes	7.495 mm
Surface Elements spacings	7.495 mm
Surface Height	29.23 cm
Surface Width	55.46 cm
Surface Area	0.16 m²
Min LOS distance between emitter and surface	3.46 m
Max LOS distance between emitter and surface	3.94 m
Average LOS distance between emitter and surface	3.69 m
Min LOS distance between surface and receiver	3.34 m
Max LOS distance between surface and receiver	3.76 m
Average LOS distance between emitter and surface	3.54 m
Min NLOS distance between emitter and receiver through surface	7.21 m
Max NLOS distance between emitter and receiver through surface	7.27 m
Average NLOS distance between emitter and receiver through surface	7.23 m
Transmitted power (in Watts)	5.00e-03 W

Transmitted power (in dBm)	6.99 dBm
Received Power (in Watts)	1.05e-04 W
Received Power (in dBm)	-9.79 dBm
Number of elements with correct reflection	965/1100
Elements with correct reflection percentage	87.73%
Original Snell's law angle (in degrees):	33.66°
Received Power without IRS (in Watts)	1.08e-10 W
Received Power without IRS (in dBm)	-69.68 dBm
Additional received power with IRS	59.89 dBm

Table 1: IRS Model Results

Finally, we can see in the Figure 16 below the complete results of our model, given by the phase shift plots (which are in in reality 2D matrices, the power plot, the visualization of the transmitter, the receiver, and the surface and finally the output of the simulation)

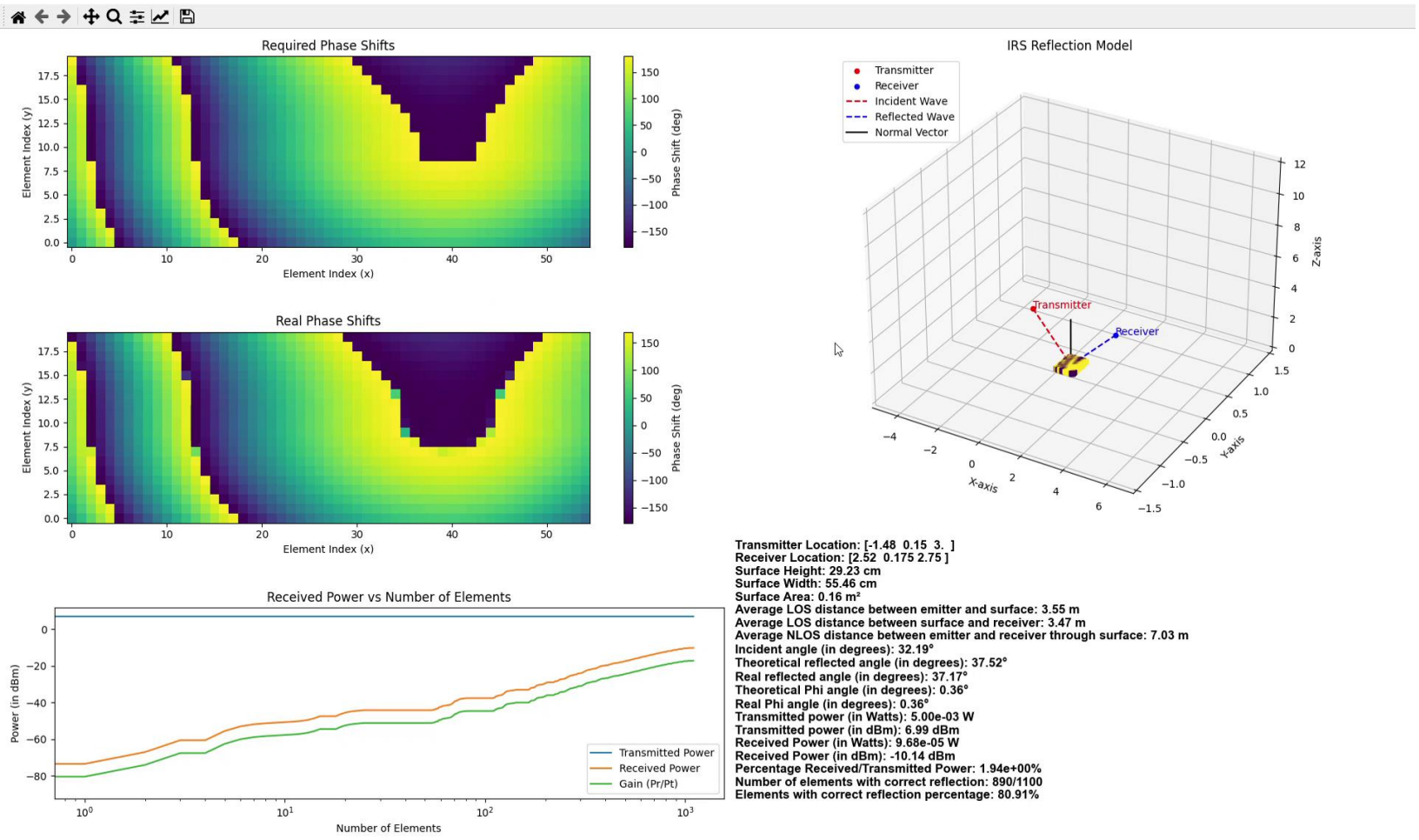

Figure 16: IRS Model Results

F. Conclusion

In this study, we embarked on an exploration of Intelligent Reconfigurable Surfaces (IRS) in the field of wireless communication systems. We started by digging into the existing knowledge available in the literature review. We found that IRS represents a revolutionary paradigm shift in wireless communication, offering the potential to enhance network performance, coverage, and capacity. The review unveiled how IRS can be employed to mitigate challenges like signal attenuation, multipath fading, and coverage dead zones. These are the primary reasons behind considering the integration of the IRS into forthcoming wireless communication frameworks like the 5^{th} and 6^{th} generation cellular networks 5G and 6G, because of its prospective capacity to address issues related to range and attenuation. We also examined recent advances in IRS applications, including beamforming, channel estimation, and interference management, illustrating the scale of its impact on the telecommunications landscape. Armed with this foundational knowledge, we set out to design a comprehensive IRS simulator based on elements with varactor diodes that could model the relation between wireless signals and intelligent surfaces. Our simulator was conceptualized to address the complex challenges of signal reflection, path optimization, and power propagation. By formulating a rigorous mathematical framework, we carefully captured the core of IRS operation, incorporating concepts from electromagnetic theory, signal processing, and geometric optics. One of the notable strengths of our simulator lies in its ability to dynamically calculate phase shifts and determine the necessary capacitance adjustments for each element of the intelligent surface. By considering the geometric properties of the environment, transmitter, and receiver, our simulator accurately simulates the reflection angles of wireless signals, enabling us to predict the efficacy of IRS deployment. The incorporation of real-world considerations, such as successful reflections and the non-line-of-sight nature of wireless communication, adds a layer of realism to the model. By employing our simulator, we were able to quantitatively demonstrate the substantial improvements that IRS brings to wireless communication systems. Through detailed calculations and comparisons, we revealed the substantial gain in received power achieved by integrating intelligent reconfigurable surfaces. This gain not only showcased the potential of IRS to revolutionize communication infrastructure but also highlighted the significance of our simulation methodology in assessing its practical impact. In conclusion, our study not only contributed to expanding the knowledge surrounding IRS but also provided a robust simulation tool to model and analyze the potential benefits of this technology. The interplay between the insights gathered from our literature review and the design of our simulator underscores the importance of a multidisciplinary approach to tackling complex challenges in wireless communication. As the field continues to evolve, our work stands as a foundation for further exploration, experimentation, and refinement of IRS applications, pushing us toward a future where intelligent surfaces reshape the landscape of wireless communication.

G. Future Work

The presented simulator model has demonstrated its capability to effectively evaluate the performance of Intelligent Reconfigurable Surfaces (IRS) in wireless communication scenarios, shedding light on their potential to enhance signal propagation and coverage. However, while our model has proven to be a valuable tool, there are several holes for future research and development that could build upon our work to further advance the field of IRS-enabled wireless communication.

Our model has predominantly focused on IRS with varactor elements, showcasing their positive impact on signal reception and coverage enhancement. However, as we observed in earlier sections, these elements may face limitations when dealing with higher frequencies, highlighting the need to focus more on IRS with elements constructed using PIN diodes, especially because our use case focuses on future 5G and 6G cellular networks with their frequencies lie in the high-end of the radio spectrum. Investigating the performance of IRS with PIN diodes at higher frequencies can provide valuable insights into their potential to address the challenges posed by the attenuation of 5G and 6G networks, thus expanding the range of applications for IRS technology.

While our work has laid the foundation for the ability of IRS to effectively redirect signals from transmitters to receivers, an important aspect that remains unexplored is bidirectionality. To fully harness the capabilities of IRS technology, it is imperative to investigate methods to enable bidirectional communication. This would empower both transmitters and receivers to exchange messages via the IRS, opening up possibilities for more dynamic and versatile wireless communication scenarios.

Furthermore, incorporating dynamic scenarios where transmitters and receivers are in motion would add a new layer of complexity. Exploring how the IRS, with bidirectionality and modulation capabilities, can adapt to the changing positions of users while maintaining optimal signal quality is a challenge that could significantly enhance the realism of our model.

Moreover, a significant aspect that deserves further exploration is the modulation of signals reflected by the IRS. With the evolution of wireless standards such as 5G and its OFDM/OFDMA modulation schemes, integrating these modulation techniques into our simulator model can provide a more realistic assessment of IRS performance. This entails studying the IRS's ability to rapidly reconfigure its elements to accommodate the specific demands of these modulation schemes, ensuring seamless and efficient communication flow for signals utilizing such modulations. Furthermore, in the context of OFDMA modulation, where multiple users simultaneously share the available bandwidth, an important topic for future work lies in enabling multiuser communication with our IRS simulator model. Investigating how the IRS can intelligently manage and optimize its reconfiguration to cater to the needs of multiple users in a dynamic and congested wireless environment, while accounting for bidirectionality and modulation, presents a complex yet rewarding research direction.

In conclusion, while our simulator model has showcased the benefits of IRS technology in wireless communication, there is still substantial work to be undertaken to fully unlock its potential. By extending our focus to IRS with different element types, enabling bidirectional communication, integrating advanced modulation techniques, accounting for dynamic user scenarios, and exploring multiuser scenarios, we can contribute to the ongoing evolution of wireless communication systems and shape the future of IRS technology.

H. Appendix

Appendix 1 : $v_{r,proj}$ Calculation :

To calculate $v_{r,proj}$ the projection of the reflected vector v_r onto the plane perpendicular to the incident plane of incidence, we will perform the following steps:

1. Find n_i the normal vector of the plane of incidence.
   We know that the incident vector v_i is inside the plane of incidence, we also know that the unit vector $u_z = [0, 0, 1]$ along the z-axis is parallel to the plane of incidence. Then to find the normal vector to the plane of incidence, we will perform the cross product of the mentioned vectors.
   $$n_i = v_i \times u_z$$
2. Find $n_{r,proj}$ the normal vector of the plane perpendicular to the plane of incidence (we will call this plane $P_{r,proj}$).
   We know that the unit vector $u_z = [0, 0, 1]$ along the z-axis is parallel to the plane $P_{r,proj}$. Additionally, since $P_{r,proj}$ is perpendicular to the plane of incidence, then the vector n_i normal to the plane of incidence will be also parallel to the plane $P_{r,proj}$. Moreover, from the previous step we know that vectors u_z and n_i are perpendicular to each other. Then the normal to the plane $P_{r,proj}$ is the vector perpendicular to both u_z and n_i. To calculate this vector, we will perform the cross product between vectors u_z and n_i.
   $$n_{r,proj} = v_i \times u_z$$
3. Calculate the projection of the reflected vector v_r onto the plane $P_{r,proj}$.
   To do so, we fist must calculate the projection of the reflected vector v_r onto the vector $n_{r,proj}$ which is the normal vector to the plane:
   $$v_{proj-v_r-n_{r,proj}} \frac{v_r \cdot n_{r,proj}}{\left|n_{r,proj}\right|^2} n_{r,proj}$$
   Then we calculate $v_{r,proj}$, the projection of the reflected vector v_r onto the plane $P_{r,proj}$:
   $$v_{r,proj} = v_r - v_{proj-v_r-n_{r,proj}}$$
   This process will be performed $w_x \times h_y$ times computing the coordinates of vector $v_{r,proj}$ the projection of the reflected vector v_r onto the plane perpendicular to the incident plane for every incident vector. So, in the end we will have a (w_x, h_y) matrix containing $v_{r,proj}$ to the corresponding incident vector v_i.

Appendix 2: Recovering the phase shift function $\phi(x, y)$

The next step is to use the $\frac{\partial \phi}{\partial x}(x, y)$ and the $\frac{\partial \phi}{\partial y}(x, y)$ matrices to find the phase shift $\phi(x, y)$ for every element of the surface. To do so, we have to start thinking in the forward direction on how the gradients are calculated before thinking how to recover the phase shift function $\phi(x, y)$ from its gradients. Then we will analyze the results of the forward thinking and apply it to the process of recovering $\phi(x, y)$.

The following equations are used to calculate the gradients of a function in both x and y direction:

In the x direction $\frac{\partial \phi}{\partial x}(x, y)$:

$$First\ column\ (x = 0): \frac{\partial \phi}{\partial x}(x, y) = \frac{\phi(x + 1, y) - \phi(x, y)}{\Delta x}$$

$$Last\ column\ (x=-1)\colon \frac{\partial \phi}{\partial x}(x,y)=\frac{\phi(x,y)-\phi(x-1,y)}{\Delta x}$$
$$Middle\ columns\ (x=[1,\dots,-2])\colon \frac{\partial \phi}{\partial x}(x,y)=\frac{\phi(x+1,y)-\phi(x-1,y)}{2\times\Delta x}$$

In the y direction $\frac{\partial \phi}{\partial y}(x,y)$:

$$First\ column\ (y=0)\colon \frac{\partial \phi}{\partial y}(x,y)=\frac{\phi(x,y+1)-\phi(x,y)}{\Delta y}$$
$$Last\ column\ (y=-1)\colon \frac{\partial \phi}{\partial y}(x,y)=\frac{\phi(x,y)-\phi(x,y-1)}{\Delta y}$$
$$Middle\ columns\ (y=[1,\dots,-2])\colon \frac{\partial \phi}{\partial y}(x,y)=\frac{\phi(x,y+1)-\phi(x,y+1)}{2\times\Delta y}$$

$\phi(x,y)$ will be a 2D array of size (w_x,h_y) as follows:

a_1	a_2	a_3	a_4	a_5	a_6	a_7	a_8	…
b_1	b_2	b_3	b_4	b_5	b_6	b_7	b_8	…
c_1	c_2	c_3	c_4	c_5	c_6	c_7	c_8	…
d_1	d_2	d_3	d_4	d_5	d_6	d_7	d_8	…
e_1	e_2	e_3	e_4	e_5	e_6	e_7	e_8	…
f_1	f_2	f_3	f_4	f_5	f_6	f_7	f_8	…
⋮	⋮	⋮	⋮	⋮	⋮	⋮	⋮	…

To be able to calculate $\phi(x,y)$ from its gradients $\frac{\partial \phi}{\partial x}(x,y)$ and $\frac{\partial \phi}{\partial y}(x,y)$, we have to fix a starting point in the $\phi(x,y)$ and used it along with the $\frac{\partial \phi}{\partial x}(x,y)$ and $\frac{\partial \phi}{\partial y}(x,y)$ values to calculate the rest of the $\phi(x,y)$ values.
So, we fix the first value of $\phi(x,y)$ and we assume it to be 0. $\phi(0,0)=0$
Now to calculate the rest of the values of the phase shifts matrix $\phi(x,y)$ we can use an altered version of the derivatives formulas as follows:

In the x direction $\frac{\partial \phi}{\partial x}(x,y)$:

$$First\ column\ (x=0)\colon \phi(x+1,y)=\left(\frac{\partial \phi}{\partial x}(x,y)\times\Delta x\right)+\phi(x,y)$$
$$Last\ column\ (x=-1)\colon \phi(x,y)=\left(\frac{\partial \phi}{\partial x}(x,y)\times\Delta x\right)+\phi(x-1,y)$$
$$Middle\ columns\ (x=[1,\dots,-2])\colon \phi(x+1,y)=\left(\frac{\partial \phi}{\partial x}(x,y)\times 2\times\Delta x\right)+\phi(x-1,y)$$

In the y direction $\frac{\partial \phi}{\partial y}(x,y)$:

$$First\ column\ (y=0)\colon \phi(x,y+1)=\left(\frac{\partial \phi}{\partial y}(x,y)\times\Delta y\right)+\phi(x,y)$$

$Last\ column\ (y=-1)$: $\phi(x,y)=\left(\frac{\partial\phi}{\partial y}(x,y)\times\Delta y\right)+\phi(x,y-1)$

$Middle\ columns\ (y=[1,\dots,-2])$: $\phi(x,y+1)=\left(\frac{\partial\phi}{\partial y}(x,y)\times 2\times\Delta y\right)+\phi(x,y-1)$

Now we will write some of the equation to calculate the elements of the phase shifts $\phi(x,y)$ matrix:

Row 1	*Column 1*
$a_1=0$	$a_1=0$
$a_2=\left(\frac{\partial\phi}{\partial x}(0,0)\times\Delta x\right)+a_1$	$b_1=\left(\frac{\partial\phi}{\partial y}(0,0)\times\Delta y\right)+a_1$
$a_3=\left(\frac{\partial\phi}{\partial x}(1,0)\times 2\times\Delta x\right)+a_1$	$c_1=\left(\frac{\partial\phi}{\partial y}(0,1)\times 2\times\Delta y\right)+a_1$
$a_4=\left(\frac{\partial\phi}{\partial x}(2,0)\times 2\times\Delta x\right)+a_2$	$d_1=\left(\frac{\partial\phi}{\partial x}(0,2)\times 2\times\Delta y\right)+b_1$
$a_5=\left(\frac{\partial\phi}{\partial x}(3,0)\times 2\times\Delta x\right)+a_3$	$e_1=\left(\frac{\partial\phi}{\partial x}(0,3)\times 2\times\Delta y\right)+c_1$
$a_6=\left(\frac{\partial\phi}{\partial x}(4,0)\times 2\times\Delta x\right)+a_4$	$f_1=\left(\frac{\partial\phi}{\partial y}(0,4)\times 2\times\Delta y\right)+d_1$

If we notice from the equations above that row 1 can be calculated uniquely starting with a_1 and using only the gradient along x; $\left(\frac{\partial\phi}{\partial x}\right)$.

Similarly, column 1 can be calculated uniquely starting with a_1 and using only the gradient along y; $\left(\frac{\partial\phi}{\partial y}\right)$.

Then by calculating the unique values of row 1 from $\frac{\partial\phi}{\partial x}$ and column 1 from $\frac{\partial\phi}{\partial y}$, we can use these values to calculates the rest of the phase shift values successively.

To calculate the other values, we will take as examples b_2 and c_3

	b_2	c_3
In x direction $\left(Using\ \frac{\partial\phi}{\partial x}\right)$	$b_2=\left(\frac{\partial\phi}{\partial x}(0{,}1)\times\Delta x\right)+b_1$	$c_3=\left(\frac{\partial\phi}{\partial x}(1,2)\times 2\times\Delta x\right)+c_1$
In y direction $\left(Using\ \frac{\partial\phi}{\partial y}\right)$	$b_2=\left(\frac{\partial\phi}{\partial y}(1,0)\times\Delta y\right)+a_2$	$c_3=\left(\frac{\partial\phi}{\partial y}(2,1)\times 2\times\Delta y\right)+a_3$

As we can see we can calculate the same value of the phase shift function in two different ways using $\frac{\partial\phi}{\partial x}$ and $\frac{\partial\phi}{\partial y}$ but in reality, there is only one phase shift function so both ways should give the same result. In other words, in order for the phase shift gradient $\frac{\partial\phi}{\partial x}$ and $\frac{\partial\phi}{\partial y}$ matrices that we have to be the gradient of the phase shift function $\phi(x,y)$, then it does not matter which gradient it is used to calculate a given value since with both we will get the same results.

After this analysis, our strategy to find the phase shifts function matrix of $\phi(x,y)$ from its gradients $\frac{\partial\phi}{\partial x}$ and $\frac{\partial\phi}{\partial y}$ is to calculate first two phase shifts matrices $\phi_x(x,y)$ and $\phi_y(x,y)$ using $\frac{\partial\phi}{\partial x}$ and $\frac{\partial\phi}{\partial y}$ respectively. Noting that in both matrices we have the same first column and first rows, where the first column is calculated starting with a_1 and using only the gradient along y; $\left(\frac{\partial\phi}{\partial y}\right)$ and the first row is calculated starting with a_1 and using only the gradient along x; $\left(\frac{\partial\phi}{\partial x}\right)$.

Theoretically after these calculations, $\phi_x(x,y)$ and $\phi_y(x,y)$ should be exacly similar to each other's, but given that we also have some imperfections when calculating initially the phase gradients $\frac{\partial\phi}{\partial x}$ and $\frac{\partial\phi}{\partial y}$, we expect some error margin which will be shown by some differences in $\phi_x(x,y)$ and $\phi_y(x,y)$. To solve this issue and to have finally one unique phase shift matrix, we will take the average of both matrices by summing them on element basis and dividing by 2. In the end, we will have the final phase shift function.

$$\phi(x,y) = \frac{\phi_x(x,y) + \phi_y(x,y)}{2}$$

This function represents the phase shift that each element should apply on the incoming signal in order to have the desired reflection. $\phi(x,y)$ will be a 2D matrix of size (w_x, h_y), where each entry represents the phase shift required to be produced by the corresponding element of the metasurface.

Appendix 3: Calculating the real reflected vector.

The first step is to find the real $v_{r,proj}$ the projection of the reflected vector v_r onto the plane perpendicular to the incident plane of incidence. We denote this plane by $P_{r,proj}$ with its normal vector $n_{r,proj}$. The coordinates of this vector will be denoted by $n_{r,proj} = [a,b,c]$

We will also denote the unit vector of the projection of the reflected vector v_r on the plane $P_{r,proj}$ by $u_{v_{pr}} = [x_{p_r}, y_{p_r}, z_{p_r}]$.

The origin of the vector $u_{v_{pr}}$ is the point with the coordinates $[x_1, y_1, z_1]$, and its extremity is the point with coordinates $[x_2, y_2, z_2]$.

Then we can also denote the vector $u_{v_{pr}} = [(x_2 - x_1), (y_2 - y_1), (z_2 - z_1)]$

We know the coordinates of the origin $[x_1, y_1, z_1]$ which are the coordinates of the element of the metasurface. Now we will be looking to find the coordinates of the extremity point of the unit vector $[x_2, y_2, z_2]$.

We also know that φ_r is the angle between $u_{v_{pr}}$ and u_z therefore we can find z_2:

$$u_{v_{pr}} \cdot u_z = z_{p_r} = \cos\ \varphi_r$$
$$z_2 - z_1 = \cos\ \varphi_r$$
$$z_2 = \cos\ \varphi_r + z_1$$

Now we can write an equation for the plane $P_{r,proj}$:

$$ax + by + cz + d = 0$$

We know that the point $[x_2, y_2, z_2]$ is in the plane $P_{r,proj}$, then we can write:

$$ax + by + cz_2 + d = 0 \quad (1)$$

This is equation 1 which will be used the find the variables $x\ and\ y$ which are basically $x_2\ and\ y_2$.

We can write this equation as:

$$y = -\frac{1}{b}(ax + cz_2 + d)$$
$$y = -\frac{1}{b}(ax + A) \qquad where\ A = cz_2 + d$$

To find the second equation we will use the formula of the norm of the vector $u_{v_{pr}}$ which is a unit vector, then we have:

$$\sqrt{{x_{p_r}}^2 + {y_{p_r}}^2 + {z_{p_r}}^2} = 1$$

$${x_{p_r}}^2 + {y_{p_r}}^2 = 1 - {z_{p_r}}^2$$
$$(x_2 - x_1)^2 + (y_2 - y_1)^2 = 1 - \cos^2\ \varphi_r$$
$$x^2 - 2x_1x + {x_1}^2 + y^2 - 2y_1y + {y_1}^2 + \cos^2\ \varphi_r - 1 = 0 \qquad (2)$$

Combining these two equations, we get:

$$x^2 - 2x_1x + {x_1}^2 + \frac{1}{b^2}(ax + A)^2 - \frac{2y_1}{b}(ax + A) + {y_1}^2 + \cos^2\ \varphi_r - 1 = 0$$
$$\left(\frac{a^2}{b^2} + 1\right)x^2 + \left(\frac{2aA}{b^2} + \frac{2ay_1}{b} - 2x_1\right)x + \left(\frac{A^2}{b^2} + \frac{2Ay_1}{b} + {x_1}^2 + {y_1}^2\cos^2\ \varphi_r - 1\right) = 0$$

Assigning the following:

$$\alpha = \frac{a^2}{b^2} + 1$$
$$\beta = \frac{2aA}{b^2} + \frac{2ay_1}{b} - 2x_1$$
$$\gamma = \frac{A^2}{b^2} + \frac{2Ay_1}{b} + {x_1}^2 + {y_1}^2\cos^2\ \varphi_r - 1$$

Now we have:

$$\alpha x^2 + \beta x + \gamma = 0$$

Solving this quadratic equation, we will have:

$$x = \frac{-\beta \pm \sqrt{\beta^2 - 4\alpha\gamma}}{2\alpha}$$

We have here 2 solutions for x, to choose between these solutions we will perform the following:
Project the receiver point $r_x = [x_r, y_r, z_r]$ onto the plane $P_{r,proj}$.
Compare the x component of the origin point x_1 of the vector $u_{v_{pr}}$, to the x component of the projection of the receiver.

$if\ x_1 > x_{r,proj}$:
$\min(sol_1, sol_2)$
$if\ x_1 < x_{r,proj}$:
$\max(sol_1, sol_2)$

now we found x. Replace it in the y equation $y = -\frac{1}{b}(ax + cz_2 + d)$
we found x_2, y_2

then we found the vector $u_{v_{pr}} = [(x_2 - x_1), (y_2 - y_1), (z_2 - z_1)]$ which is the unit vector of the vector $v_{r,proj}$ that we are looking for. To find this vector from its unit vector, first we have to write $u_{v_{pr}}$ in parametric form:

$x = x_1 + (x_2 - x_1)t$
$y = y_1 + (y_2 - y_1)t$
$z = z_1 + (z_2 - z_1)t$

We are looking for the point of the vector that is on the plane of the receiver, in other words, we are looking for the point on the line having unit vector $u_{v_{pr}}$ where $z = z_{receiver}$

$$t = \frac{z_{receiver} - z_1}{(z_2 - z_1)}$$

Now we replace this t in the equations of x and y to find their values.

Finally, we can find the reflected vector $v_{r,proj} = [(x - x_1), (x - y_1), (z_{receiver} - z_1)]$

After finding the projection of the reflected vector $v_{r,proj}$, the next step is to find the reflected vector v_r using its reflection $v_{r,proj}$.

In this section we consider $v_{r,proj} = [a, b, c]$

The reflected vector $v_r = [x, y, z]$

We want to find the coordinates $[x, y, z]$ of the reflected vector v_r

We also know that the z coordinate of the vectors $v_{r,proj}$ and v_r will be the same: $z = c = z_r$

We also know that $|v_{r,proj}| = |v_r| \cos\theta_r$

$$\Rightarrow |v_r| = \frac{|v_{r,proj}|}{\cos\theta_r} = L$$

$$|v_r| = \sqrt{x^2 + y^2 + z_r^2} = L$$

$$x^2 + y^2 + z_r^2 - L^2 = 0 \qquad (1)$$

This is equation 1 used to find the reflected vector $v_r = [x, y, z]$

To find the second equation we will use the dot product between $v_{r,proj}$ and v_r

$$v_{r,proj} \cdot v_r = ax + by + cz = |v_{r,proj}||v_r| \cos\theta_r$$
$$ax + by + z^2 = |v_{r,proj}||v_r| \cos\theta_r$$
$$ax + by = |v_{r,proj}||v_r| \cos\theta_r - z^2$$
$$ax + by = X \qquad where\ X = |v_{r,proj}||v_r| \cos\theta_r - z^2$$

$$\Rightarrow y = \frac{X - ax}{b} \qquad (2)$$

Combining equations (1) and (2):

$$x^2 + \frac{1}{b^2}(X - ax)^2 + {z_r}^2 - L^2 = 0$$

$$x^2 + \frac{X^2}{b^2} + \frac{a^2}{b^2}x^2 - \frac{2Xa}{b}x + {z_r}^2 - L^2 = 0$$

$$\left(\frac{a^2}{b^2} + 1\right)x^2 - \frac{2Xa}{b}x + \left(\frac{X^2}{b^2} + {z_r}^2 - L^2\right) = 0$$

Assigning the following:

$\alpha = \frac{a^2}{b^2} + 1$

$\beta = -\frac{2Xa}{b}$

$\gamma = \frac{X^2}{b^2} + {z_r}^2 - L^2$

Now we have:

$$\alpha x^2 + \beta x + \gamma = 0$$

Solving this quadratic equation, we will have:

$x = \frac{-\beta \pm \sqrt{\beta^2 - 4\alpha\gamma}}{2\alpha}$

We have here 2 solutions for x, to choose between these solutions we will perform the following:

$est_{sol_1} = sol_1 + x_0$

$est_{sol_2} = sol_2 + x_0$

Where x_0 is the x component of the origin of the reflected vector which is known (the x coordinate of the element of the metasurface).

Then we choose the solution which is closer to the x coordinate of the receiver, $x_{receiver}$.

$if\ |est_{sol_1} - x_{receiver}| > |est_{sol_2} - x_{receiver}|$:

sol_1

$else$:

sol_2

now we found x. Replace it in the y equation $y = \frac{|v_{r,proj}||v_r|\cos\theta_r - z^2 - ax}{b}$

we found x, y of the reflected vector $v_r = [x, y, z_r]$

then to find the extremity point of this vector, or the point that will hit the plane of the receiver, we will do the following:

$p_r = [(x + x_1), (y + y_1), (z_r + z_1)]$

$p_r = [x_{pr}, y_{pr}, z_{pr}]$

where the point$[x_1, y_1, z_1]$ is the origin of the reflected vector, which is the coordinates of point center of the element on the metasurface.

Appendix 4: Calculating the incident angle θ_i based in the original Snell's law $\theta_r = \theta_i$

Given the location of the transmitter $t_x = [x_i, y_i, z_i]$, the location of the receiver $r_x = [x_r, y_r, z_r]$, the normal to the plane of incidence, (considering our initial assumption for a fixed coordinates system where the transmitter and the receiver are points in space, and the surface of incidence in the x-y plane, (z=0) so the normal is the unit vector parallel to the z-axis $u_z = [0, 0, 1]$) we can calculate the angles θ_r and θ_i so a transmitted ray reaches the receiver.

We define the location of incidence at point $p_0\ (x, y)$. We have to find p_0.

$Incidence\ vector$: $v_i = [(x_i - x), (y_i - y), z_i]$

$Reflected\ vector$: $v_r = [(x - x_r), (y - y_r), z_r]$

Then we have:

$$v_i \cdot u_z = z_i$$
$$= |v_i||u_z| \cos\theta_i$$
$$\Rightarrow \theta_i = \cos^{-1}\left(\frac{v_i \cdot u_z}{|v_i||u_z|}\right) = \cos^{-1}\left(\frac{z_i}{|v_i||u_z|}\right)$$

and

$$v_r \cdot u_z = z_r$$
$$= |v_r||u_z| \cos\theta_r$$
$$\Rightarrow \theta_r = \cos^{-1}\left(\frac{v_r \cdot u_z}{|v_r||u_z|}\right) = \cos^{-1}\left(\frac{z_r}{|v_r||u_z|}\right)$$

$$\theta_i = \theta_r$$

$$\cos^{-1}\left(\frac{z_i}{|v_i||u_z|}\right) = \cos^{-1}\left(\frac{z_r}{|v_r||u_z|}\right)$$

$$\frac{z_i}{|v_i|} = \frac{z_r}{|v_r|}$$

$$\frac{z_i}{\sqrt{(x_i - x)^2 + (y_i - y)^2 + {z_i}^2}} = \frac{z_r}{\sqrt{(x - x_r)^2 + (y - y_r)^2 + {z_r}^2}}$$

$$\frac{(x_i - x)^2 + (y_i - y)^2 + {z_i}^2}{(x - x_r)^2 + (y - y_r)^2 + {z_r}^2} = \left(\frac{z_i}{z_r}\right)^2$$

$$\frac{(x_i - x)^2 + (y_i - y)^2 + {z_i}^2}{(x - x_r)^2 + (y - y_r)^2 + {z_r}^2} - \left(\frac{z_i}{z_r}\right)^2 = 0$$

Then we should find the point $p_0\ (x, y)$ so the function above is closest to 0.

After finding the point $p_0\ (x, y)$, to find the angles $\theta_i = \theta_r$:

$v_i = t_x - p_0$

$\theta_i = \cos^{-1}\left(\frac{v_i \cdot u_z}{|v_i||u_z|}\right)$

Code Repository

https://gitlab.inria.fr/fantastic-fanfare/IntelligentReconfigurableSurfaces.git

References:

[1] J. Gros, “A Reconfigurable Intelligent Surface at mmWave Based on a Binary Phase Tunable Metasurface,” vol. 2, no. April, pp. 1055–1064, 2021.

[2] Q. Wu, S. Zhang, B. Zheng, C. You, and R. Zhang, “Intelligent Reflecting Surface-Aided Wireless Communications: A Tutorial,” *IEEE Trans. Commun.*, vol. 69, no. 5, pp. 3313–3351, 2021.

[3] E. Björnson, H. Wymeersch, B. Matthiesen, and P. Popovski, “Intelligent Surfaces,” 2022.

[4] H. Zhang and B. Di, “Reconfigurable Intelligent Surfaces Assisted Communications With Limited Phase Shifts : How Many Phase Shifts Are Enough ?,” *IEEE Trans. Veh. Technol.*, vol. 69, no. 4, pp. 4498–4502, 2020.

[5] E. Basar *et al.*, “Reconfigurable Intelligent Surfaces,” *IEEE Access*, vol. PP, no. June 2018, p. 1, 2019.

[6] P. Pirinen, “A brief overview of 5G research activities,” *Proc. 2014 1st Int. Conf. 5G Ubiquitous Connect. 5GU 2014*, pp. 17–22, 2014.

[7] H. E. S. Jöland, S. M. Ieee, F. R. T. Ufvesson, and F. Ieee, “6G Wireless Systems : Vision , Requirements , Challenges , Insights , and Opportunities,” *Proc. IEEE*, vol. 109, no. 7, pp. 1166–1199, 2021.

[8] S. Elmeadawy and R. M. Shubair, “6G Wireless Communications : Future Technologies and Research Challenges,” pp. 5–9, 2019.

[9] M. Di Renzo *et al.*, “Smart Radio Environments Empowered by Reconfigurable Intelligent Surfaces: How It Works, State of Research, and the Road Ahead,” *IEEE J. Sel. Areas Commun.*, vol. 38, no. 11, pp. 2450–2525, 2020.

[10] Y. Liu *et al.*, “Reconfigurable Intelligent Surfaces : Principles and Opportunities,” no. c, pp. 1–33, 2021.

[11] M. A. Elmossallamy, H. Zhang, L. Song, K. G. Seddik, Z. Han, and G. Y. Li, “Reconfigurable Intelligent Surfaces for Wireless Communications: Principles, Challenges, and Opportunities,” *IEEE Trans. Cogn. Commun. Netw.*, vol. 6, no. 3, pp. 990–1002, 2020.

[12] X. Pei *et al.*, “RIS-Aided Wireless Communications : Prototyping , Adaptive Beamforming , and Indoor / Outdoor Field Trials,” pp. 1–13.

[13] L. Sanguinetti, “Power Scaling Laws and Near-Field Behaviors of Massive MIMO and Intelligent Reflecting Surfaces,” vol. 1, no. July, 2020.

[14] “CONVERGE – Telecommunications and Computer Vision Convergence Tools for Research Infrastructures,” vol. 1, no. 1, pp. 1–45.

[15] A. L. I. Araghi and G. S. Member, “Reconfigurable Intelligent Surface (RIS) in the Sub-6 GHz Band : Design , Implementation , and Real-World Demonstration,” *IEEE Access*, vol. 10, pp. 2646–2655, 2022.

[16] H. Kamoda, T. Iwasaki, J. Tsumochi, T. Kuki, and O. Hashimoto, “60-GHz electronically reconfigurable large reflectarray using single-bit phase shifters,” *IEEE Trans. Antennas Propag.*, vol. 59, no. 7, pp. 2524–2531, 2011.

[17] Y. Cui, H. Yin, L. Tan, and M. Di Renzo, “A 3D Positioning-based Channel Estimation Method for RIS-aided mmWave Communications,” pp. 1–11, 2022.

[18] H. Yang, X. Cao, F. Yang, J. Gao, S. Xu, and M. Li, “OPEN A programmable metasurface with dynamic polarization , scattering and focusing control,” *Nat. Publ. Gr.*, no. October, pp. 1–11, 2016.

[19] X. Tan, Z. Sun, D. Koutsonikolas, and J. M. Jornet, “Enabling Indoor Mobile Millimeter-wave Networks Based on Smart Reflect-arrays,” *Proc. - IEEE INFOCOM*, vol. 2018-April, pp. 270–278, 2018.

[20] R. Fara, P. Ratajczak, A. Ourir, M. Di Renzo, and J. De Rosny, “6G : THE PARADIGM FOR FUTURE WIRELESS COMMUNICATIONS A Prototype of Reconfigurable Intelligent Surface with Continuous Control of the Reflection Phase,” no. February, pp. 70–77, 2022.

[21] E. Björnson and L. Sanguinetti, “DEMYSTIFYING THE POWER SCALING LAW OF,” pp. 549–553, 2019.

[22] K. Wang, C. T. Lam, and B. K. Ng, “On hardware aging for practical RIS-assisted communication systems,” *Electron. Lett.*, vol. 59, no. 2, 2023.

[23] E. Basar, I. Yildirim, and F. Kilinc, “Indoor and Outdoor Physical Channel Modeling and Efficient Positioning for Reconfigurable Intelligent Surfaces in mmWave Bands,” *IEEE Trans. Commun.*, vol. 69, no. 12, pp. 8600–8611, 2021.

[24] F. Liu *et al.*, “Intelligent Metasurfaces with Continuously Tunable Local Surface Impedance for Multiple Reconfigurable Functions,” *Phys. Rev. Appl.*, vol. 11, no. 4, p. 1, 2019.

[25] V. Popov, M. Odit, J. Gros, V. Lenets, and A. Kumagai, “Experimental Demonstration of a mmWave Passive Access Point Extender Based on a Binary Recon fi gurable Intelligent Surface,” vol. 2, no. October, pp. 1–8, 2021.

[26] C. G. Liu, E. T. Zhang, Z. P. Wu, and B. Zhang, “Modelling radio wave propagation in tunnels with ray-tracing method,” *2013 7th Eur. Conf. Antennas Propagation, EuCAP 2013*, pp. 2317–2321, 2013.

[27] S. Abeywickrama, S. Member, R. Zhang, and Q. Wu, “Intelligent Reflecting Surface : Practical Phase Shift,” vol. 68, no. 9, 2020.

[28] Ö. Özdogan, S. Member, E. Björnson, S. Member, and E. G. Larsson, “Intelligent Reflecting Surfaces : Physics , Propagation , and Pathloss Modeling,” no. 2, pp. 1–5.

[29] A. M. H. Wong and G. V. Eleftheriades, “Perfect Anomalous Reflection with a Bipartite Huygens’ Metasurface,” *Phys. Rev. X*, vol. 8, no. 1, 2018.

[30] L. Dai *et al.*, “Reconfigurable Intelligent Surface-Based Wireless Communications: Antenna Design, Prototyping, and Experimental Results,” *IEEE Access*, vol. 8, pp. 45913–45923, 2020.

[31] B. Rana, “Review Paper on Hardware of Reconfigurable Intelligent Surfaces,” *IEEE Access*, vol. 11, no. February, pp. 29614–29634, 2023.

[32] R. I. S. T. Alliance, “Reconfigurable Intelligent Surface Technology White Paper,” no. March, 2023.

[33] Y. Zhou *et al.*, “Design of Phase Gradient Coding Metasurfaces for Broadband Wave Modulating,”

Sci. Rep., vol. 8, no. 1, pp. 1–9, 2018.

[34] M. Di Renzo *et al.*, “Smart radio environments empowered by reconfigurable AI meta-surfaces : an idea whose time has come,” 2019.

[35] N. Yu, F. Capasso, and Z. Gaburro, “Light Propagation with Phase Reflection and Refraction,” vol. 333, no. 2011, 2012.

[36] N. Yu *et al.*, “Flat Optics : Controlling Wavefronts With Optical Antenna Metasurfaces,” vol. 19, no. 3, 2013.

[37] M. K. T. Al-Nuaimi, W. Hong, and X. Gao, “1D and 2D phase gradient perforated dielectric reflective surfaces at mmWave,” *Int. J. Microw. Wirel. Technol.*, vol. 10, no. 4, pp. 446–452, 2018.

[38] F. Aieta, P. Genevet, N. Yu, M. A. Kats, Z. Gaburro, and F. Capasso, “Out-of-plane reflection and refraction of light by anisotropic optical antenna metasurfaces with phase discontinuities,” *Nano Lett.*, vol. 12, no. 3, pp. 1702–1706, 2012.

[39] O. S. a. B. D. Larry Peterson, Private 5G: A Systems Approach, Systems Approach LLC, 2023.

[40] F. G. V. W. Jean-Louis Coutaz, Principles of Terahertz Time-Domain Spectroscopy, Jenny Stanford Publishing, 2018, p. 640.